AN EXPERIMENTAL STUDY ON SINGLE CRYSTAL DIAMOND TURNING OF OPTICAL QUALITY SILICON

A THESIS SUBMITTED TO
THE GRADUATE SCHOOL OF NATURAL AND APPLIED SCIENCES
OF
MIDDLE EAST TECHNICAL UNIVERSITY

BY

SERDAL ÇALI

IN PARTIAL FULFILLMENT OF THE REQUIREMENTS
FOR
THE DEGREE OF MASTER OF SCIENCE
IN
MECHANICAL ENGINEERING

JANUARY 2008

Approval of the thesis:

AN EXPERIMENTAL STUDY ON SINGLE CRYSTAL DIAMOND TURNING OF OPTICAL QUALITY SILICON

submitted by **SERDAL ÇALI** in partial fulfillment of the requirements for the degree of **Master of Science in Mechanical Engineering Department, Middle East Technical University** by

Prof. Dr. Canan Özgen _____
Dean, Graduate School of **Natural and Applied Sciences**

Prof. Dr. Kemal Ider _____
Head of the Department, **Mechanical Engineering**

Prof. Dr. Mustafa İlhan Gökler _____
Supervisor, **Mechanical Engineering Dept., METU**

Examining Committee Members:

Prof. Dr. Demir Bayka _____
Mechanical Engineering Dept., METU

Prof. Dr. Mustafa İlhan Gökler _____
Mechanical Engineering Dept., METU

Prof. Dr. S.Engin Kılıç _____
Mechanical Engineering Dept., METU

Prof. Dr. Metin Akkök _____
Mechanical Engineering Dept., METU

Tolga Ziya Sander (M.Sc.) _____
Design Leader, ASELSAN

Date: 03.01.2008

I hereby declare that all information in this document has been obtained and presented in accordance with academic rules and ethical conduct. I also declare that, as required by these rules and conduct, I have fully cited and referenced all material and results that are not original to this work.

Name, Last Name: Serdal Çalı

Signature:

ABSTRACT

AN EXPERIMENTAL STUDY ON SINGLE CRYSTAL DIAMOND TURNING OF OPTICAL QUALITY SILICON

Çalı, Serdal

M.Sc., Department of Mechanical Engineering

Supervisor: Prof. Dr. Mustafa İlhan Gökler

January 2008, 102 pages

Silicon is commonly used in infrared (IR) imaging systems. The surface quality is an important issue in optics manufacturing since surface roughness affects optical performance of imaging systems. Surface quality of an optical component is determined by number of factor, including cutting parameters; cutting speed, depth of cut and feed in radial direction.

In this thesis, an experimental study has been performed to investigate the relation between cutting parameters and average roughness of the surface of silicon. In the experiments, silicon specimens, which have a diameter of 50 mm, were face turned by using a 2-axis CNC single point diamond turning machine. The specimens were machined by using either constant spindle speed or constant cutting speed. Two different tools with rake angles of -15 degrees and -25 degrees were used. The attained surfaces were measured by using a white light interferometer, which has a resolution of 0.1nm.

The experiments were designed according to the “factorial design” method, considering cutting parameters. The effects of cutting parameters and tool rake angles on surface quality of silicon were observed. The best average surface roughness obtained was about 1 nm which is quite better than the acceptable average surface roughness level of 25 nm.

Keywords**:** Ultraprecision Machining, Silicon, Optics, Surface Roughness, Design of Experiment

ÖZ

OPTİK KALİTEDE SİLİKONUN TEK KRİSTAL ELMAS İLE TORNALANMASININ DENEYSEL OLARAK İNCELENMESİ

Çalı, Serdal
Yüksek Lisans, Makina Mühendisliği Bölümü
Tez Yöneticisi: Prof. Dr. Mustafa İlhan Gökler

Ocak 2008, 102 sayfa

Silikon kızılötesi görüntüleme sistemlerinde yaygın olarak kullanılmaktadır. Bu sistemlerdeki optik elemanların yüzey kalitesi, cihazların performansı açısından önemli bir kriter olarak değerlendirilir. Tornalanarak elde edilen optik yüzeylerde; kesme parametreleri ve takım geometrisi yüzey pürüzlülüğü açısından belirleyici faktörler arasındadır.

Bu çalışmada kesme parametreleri ile ortalama yüzey pürüzlülüğü Ra arasında bir ilişki incelenmiştir. 50 mm çağlı silikon yüzeyler, değişik kesme parametreleri kullanılarak tornalanmıştır. Kullanılan tezgah 2-eksenli CNC bir tornadır. Deneylerde, silikon yüzeyler sabit devirde yada sabit kesme hızında işlenmiştir. Deneyler esnasında kullaılan takımların talaş açıları -15 derece ve -25 derece olarak değiştirilmiştir. İşlenen yüzeyler, 0.1 nm çözünürlüklü bir interferometere ile ölçülerek Ra değerleri elde edilmiştir.

Deney tasarımı “faktoriyel tasarım” esasları kullanılarak yapılmıştır. Yapılan çalışma sonucunda kesme parametrelerinin ve talaş açısının yüzey pürüzlülüğü üzerindeki etkisi incelenmiştir. Lineer bir regresyon modeli elde edilerek belirli koşullar altında Ra değerinin öngörülmesini sağlayan bir formül elde edilmiştir. Bunların yanısıra, silikon malzenin işlenmesinde kristal yöneliminin etkisi gözlenmiştir. Elde edilen en iyi Ra değeri yaklaşık olarak 1 nm olup, kabul edilebilir üst sınır olan 25 nm’nin çok altındadır

Anahtar Sözcükler: Hassa tornalama,Silicon, Optik, Yüzey Pürüzlülüğü, Deney Tasarımı

To My Family

ACKNOWLEDGEMENTS

I would like to sincerely thank my supervisor, Prof. Dr. Mustafa İlhan Gökler, for his guidance, advice and encouragement throughout the study.

I wish to thank Prof. Dr. Engin Kılıç and Prof. Dr. Ömer Anlağan, for their valuable interpretations and advices.

I also wish to thank ASELSAN, Inc. and my manager in ASELSAN, Mr. İhsan Özsoy, for his support and providing me the facility in this work. I express my sincere thanks to Mr. Tolga Sander for his valuable supports and advices in my study. And, I would like to thank Dr. Devrim Anıl for his support and help. Technical assistance of Mr. İlker Sezen is gratefully acknowledged.

I offer my thanks to Mr. Hacı Batman and Mr. Enver Çağırıcı in Main Maintenance Base, Adapazarı.

I would also like to offer my deepest thanks to my parents for their support, encouragement and faith in me, throughout my life.

Last, but certainly not least, I would like to thank my wife, for her love and support during some very stressful times. I would have never made it through without her.

TABLE OF CONTENTS

LIST OF TABLES

TABLES

LIST OF FIGURES

FIGURES

LIST OF SYMBOLS

SYMBOL

A_c	: Cross sectional area of uncut chip
d	: Depth of cut
D	: Diameter
f	: Feed
fr	: Feedrate
l_w	: Length of workpiece
N	: Rotational speed
Ra	: Average roughness
Rp	: Maximum peak height
Rq	: Root mean square roughness
Rv	: Maximum valley depth
Rz	: Maximum peak-to-valley height
t	: Chip thickness
t_c	: Critical chip thickness
t_m	: Machining time
V	: Cutting speed
V_{av}	: Average cutting speed
Z_w	: Material removal rate

CHAPTER 1

INTRODUCTION

1.1 Use of Thermal Imaging Systems

Thermal imaging systems have growing utilization in different areas. Military, law enforcement, hunting, observation of wild, security, hidden objects detection, entertainment and medical can be counted as usage areas of thermal imaging systems. However, usage of thermal imaging systems is more vital for military application than the others. Reconnaissance, surveillance and aiming at night conditions are the main requirements of military for these devices. Some of Aselsan Inc. thermal imaging products for military applications are shown in Figures 1.1- 1.3.

Police uses thermal systems mostly only for surveillance for law enforcement. Besides, in order to determine the place where a victim is buried, thermal systems are used as well.

Figure 1.1 ASELFLIR-200 Airborne Thermal Imaging System [1]
(Courtesy of ASELSAN)

Hunters sometimes aim with thermal sights, which can be bought in the market or at least pursue their hunts in darkness.

Figure 1.2 ASIR Thermal Imaging System [1]
(Courtesy of ASELSAN)

Figure 1.3 Thermal Weapon Sight [1]
(Courtesy of ASELSAN)

Although, most of the applications are focused on military requirement, civilian applications are also increasing. In medical field, cancer cells are sought by making use of thermal imaging applications. In Figure 1.4, a group of cancer cells is figured out and can be seen as white region. It is clearly seen that the region

around the cancer cells is hotter than the other parts of the body. An industrial application is carried out by the car manufacturing company BMW [2]. As seen in Figure 1.5, the driver is more aware of the surrounding of the car by using the thermal view provided by the thermal imaging system installed in the car.

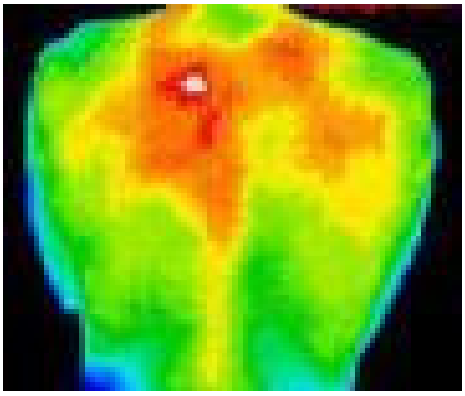

Figure 1.4 Medical Applications of Thermal Imaging Systems

Figure 1.5 Thermal Camera Usage in BMW [2]

1.2 Working Principles of Thermal Imaging Systems

Naked human eye can see a very small portion of the electromagnetic waves around us. Electromagnetic spectrum, which is given in Figure 1.6, covers all the rays in the universe. The visible part of electromagnetic spectrum starts from 370 nm and ends at 720 nm. Below 370 nm, there exist ultraviolet (UV) radiation, X-rays and gamma rays. Beyond 720 nm, infrared (IR) radiation, microwave, radio rays take place.

Even tough, with naked eyes we can only see a very small range of the electromagnetic spectrum, by making use of some instrument; it is possible to visualize things that we cannot see. Thermal imaging systems utilize infrared range of electromagnetic spectrum.

Infrared spectrum extends from 0.72 μm, which is the boundary of the visible light, to 1000 μm, which is the boundary of the microwaves. IR band is situated between the visible light and the microwave band. Therefore some properties of IR seem like visible and some other microwave. IR radiation can be focused or reflected like visible light, on the other side, it can be transmitted to long distances like microwave radiation [3]. IR band is divided into three sub-bands because different type of devices is optimized for each part of the IR band. The subdivisions in IR spectrum are given as

- Near IR : 0.7 μm to 1.3 μm
- Middle IR : 1.3 μm to 5.6 μm
- Far IR : 5.6 μm to 1000 μm

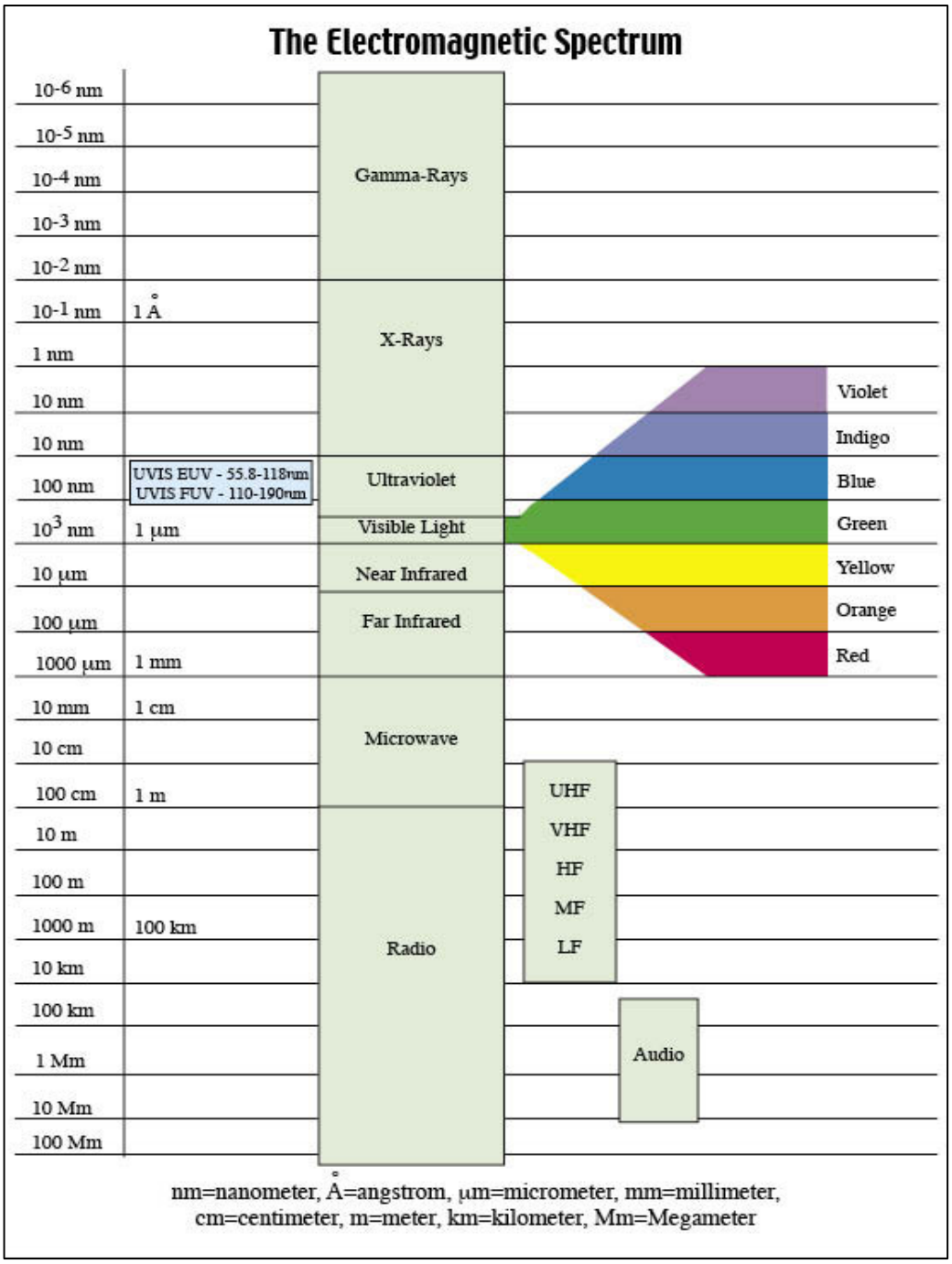

Figure 1.6 Electromagnetic Spectrum [4]

The living and non-living objects emit most of their thermal radiations in the range of 3-5 μm and 8-12 μm, respectively. These are the tactical and natural target for military applications [5]. Thermal imaging systems use these parts of energy received from environment and transforms this energy to image. Since any object always emits IR energy, thermal imaging system can be employed during day and night. Besides, snow, fog or rain do not prevent using systems.

The main elements of a thermal system, which is used in a military application, are depicted in Figure 1.7. The IR energy of the targets is received by the imaging system. Some optical components like windows, lenses and mirrors make the IR light follow a predefined path and focus on the detector. The detector transfers the information brought by the IR light into electrical signals. The signals are processed by the image processing unit and fed to the monitor.

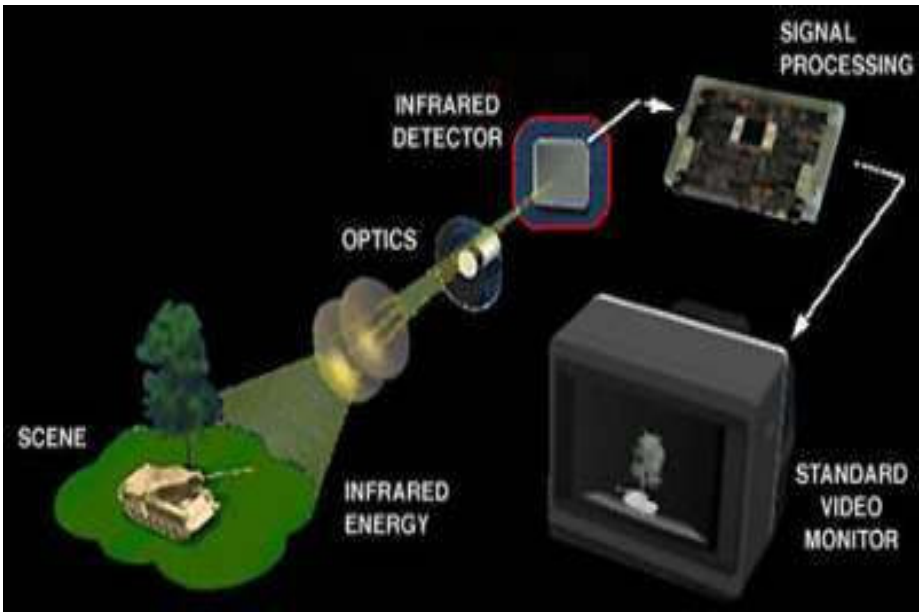

Figure 1.7 Basic Elements of Thermal Imaging Systems [6]

1.3 Optical Components in Thermal Imaging Systems

The optical components in thermal imaging systems are similar with the optics used in daylight. However, the optics in IR systems is made materials which have a high transmission for IR energy. The most common materials employed in this field are germanium and silicon.

Properties of silicon and germanium are given in Table 1.1. Comparing mechanical properties of silicon and germanium, it can be stated that the density of silicon is less than half of density of the germanium. This is especially important for military applications in which weight is a constraint. Young modulus and shear modulus of both do not differ so much. Silicon is harder than germanium and has higher melting point. Thermal expansion coefficient of silicon is lower than that of germanium. This property makes the design with silicon more stable. In addition, silicon has a better transmission in the range of 3-5 μm. The transmission curves of silicon and germanium are given in Figures 1.8-1.9.

Table 1.1 Properties of Silicon and Germanium [7]

Property	Unit	Silicon	Germanium
Density	gr/cm^3	2,32	5,32
Young Modulus	GPa	112,4	130
Shear Modulus	GPa	43,9	50
Hardness(Vickers)	N/mm^2	11270	7644
Poisson's Ratio	-	0.38	0,3
Meting Point	°C	1420	937,4
Refractive Index @589nm	-	3,49	3,99
Thermal Expansion @20°C	μm/m°C	2,49	6,1
Thermal Conductivity	W/mK	124	64

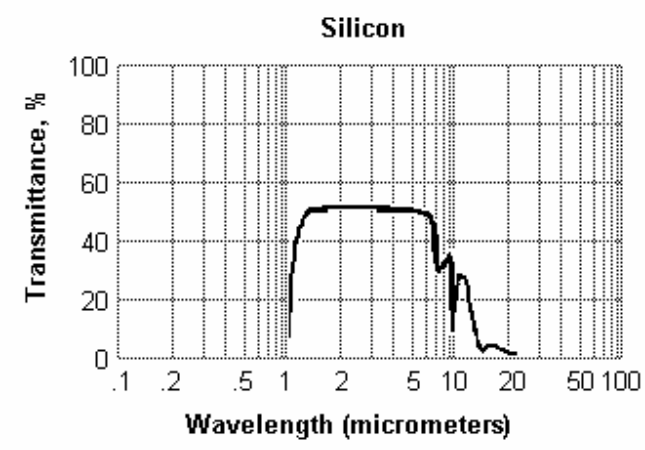

Figure 1.8 Transmittance of Silicon in the Spectrum [8]

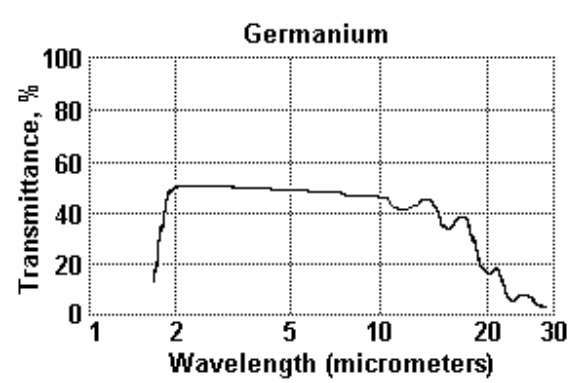

Figure 1.9 Transmittance of Germanium in the Spectrum [8]

1.4 Production of Silicon Optics

Conversion of silicon ingots into optics or wafers in electronics industry requires some machining operations. In the electro-optics industry lenses and mirrors are traditionally fabricated by multiple processes; grinding, lapping and polishing. However, this production method is time consuming and costly. Besides, only simple profiles such as spherical and flat shapes are possible. The alternative

method for these manufacturing steps is single point diamond turning (SPDT) [9]. Detailed information on SPDT is given in Chapter 2.

1.5 Previous Studies

In 1991 Ikawa et al. [10] presented a review on ultra precision metal cutting technology which is aiming micrometer or sub micrometer form accuracy and nanometric surface roughness in optical, electronic and mechanical components. It is stated that, historically, the ultra precision metal cutting in the present sense had begun to be investigated in the 1960's with the demand in advanced science and technology for energy, computer, electronics and defense applications. The Lawrence Livermore National Laboratory carried out the pioneering works in the field. In 1970's the experimental work was performed in its application to optical components of complex forms. In 1980's , these excessive efforts have resulted in the developments of highly advanced machine tools with sophisticated metrology and control of diamond tools of reliable quality.

Ju and Yan [11] presented their study on ultra precision diamond turning of optical crystals in 1994. In the study, the main factors influencing the machined surface quality were reported. It is stated that cutting speed has no obvious influence on machined surface quality and low feed rate of the cutting tool is essential to ductile cutting of brittle materials. They demonstrated that, brittle optical crystals can be machined by ductile regime cutting, which is described in Chapter 2, under the optimized cutting conditions and therefore fine optical surfaces can be obtained.

Fang in 1997 [12] obtained high quality silicon surfaces by single point diamond turning. Surface integrity and cutting conditions were analyzed in this work. The experimental study was performed by making use of a Precitech ultra precision machine, Optimum 2800. The surface roughness values were measured with an

interferometric surface analysis microscope, Zygo. It is reported that at a depth of cut of 1µm, a feed of 4 mm/ min, and a cutting speed of 80 m/min, a mirror surface of roughness R_a of 5.9 nm was obtained. Furthermore, decreasing this feed rate 10 times to 0.4 mm/min gives a roughness of R_a equals to 1 nm.

Fang and et.al gave away another experimental study in 1998 [13]. In this work they tried different tools with rake angles of 0° and -25° at different cutting speeds and different depth of cut on silicon. Mirror surface of R_a=1 nm roughness is achieved where a depth of cut of 1µm, feedrate of 0.4 mm/min and a cutting speed of 90 m/min. It is claimed that these parameters satisfied ideal ductile cutting conditions.

Xiangdong [9] presented a technical report in 2000 and published his experimental result on single point diamond turning of different optical materials. One of the materials investigated was silicon. He stated that machining in ductile mode is important to produce optical quality surfaces on brittle materials. However, he added that "the basic physical mechanism underlying the ductile-regime machining is not fully understood". In this, work mirror surfaces with 1 nm roughness were achieved by a depth of cut of 1µm, feedrate of 0.4 mm/min and a cutting speed of 80 m/min. The tool had a rake angle of 0° and a radius of 0.5 mm. The tool was waviness controlled. In experimentation Precitech – Optimum 4200 ultra precision lathe was utilized.

Machining silicon and germanium similarly has some challenges due to being a brittle material. This condition of these materials has been the subject of some studies. Morris and Callahan (1995) [14] investigated ductile regime single point diamond turning of brittle materials such as silicon and germanium. They concluded that machining parameters such as large negative rake angles, sharp

cutting edges and small depths of cut help to promote ductile behaviors in brittle materials.

Another research on ductile regime cutting was by Leung et.al in 1998 [15]. They investigated the effects of cutting parameters and diamond tool rake angle. They turned their specimen at a spindle speed of 10000 rpm and three different depth of cut; 1, 5, 10 µm and two different feedrate such as 10, 20 mm/min. They stated that the best surface is attained at a depth of cut of 1µm and a feed of 1 µm/rev. The achieved R_a was 2.86 nm.

Blake et.al [16] have prior studies on ductile regime machining of silicon and germanium. They brought out that silicon and germanium can be diamond turned in a regime where material removal was by plastic flow without introduction of fracture into the surface. They defined a critical chip thickness above which the damage created by a tool pass could not be cleaned up by subsequent passes. Their work showed that, the critical chip thickness is a function of feed rate, crystal orientation and tool rake angle but it is relatively insensitive to cutting speed. In addition, it was shown experimentally that as the rake angle became more negative, the resulting critical chip thickness increased.

Ductile regime machining is an important point in silicon machining. Ductile cutting of brittle materials is explained by Sreejith et.al [17, 18]. In these studies, it is stated that, ductile regime cutting can be argued from a consideration of material removal energy. Ductile regime occurs if the energy required for plastic deformation is lower than the energy needed for fracture. Besides, it is affirmed that a Ra of 1 nm was attained with a depth of cut of 1 nm, feedrate of 0.4 mm/min and a cutting speed of 400 m/min in single point diamond turning.

Furthermore, the transition of material removal from brittle to ductile was observed by Zhou et.al in 2002 [19]. They observed the transition by continuously changing the cutting depth. It is shown that the mode of material deformation can shift from brittle to ductile when the depth of cut is less than a critical value. For generating optical surfaces on brittle materials by using the diamond cutting process, the selection of tool geometry and machining parameters are important if the work material is to be deformed in ductile mode. Besides the tool rake angles influence the brittle-ductile transition in diamond cutting of silicon single crystals. The surface quality generated with a tool of -25° rake angle is much better than that produced with a tool of 0° rake angle.

Yan et.al [20] performed a study on ductile regime turning of silicon substrates. They proposed ductile regime turning using a sharp nosed diamond instead of a round nosed diamond tool. They stated that adopting a very small cutting edge enables ductile regime turning at a large tool feed up to a few tens of micrometers. The investigation was performed by making use of a Toyoda ultra precision lathe and the surfaces of the specimens were measured with a Form Talysurf device. The cutting parameters were selected as spindle speed of 1500 rpm, depth of cut 1 µm and feed of 100 µm/ rev. The resulting surface roughness was obtained as R_a=7.3 nm.

Chao et al. [21] studied ductile regime machining of silicon. They concluded that under some chosen cutting conditions, it is possible to machine silicon ductile manner. However, silicon machining is orientation dependent. In their work, it is shown that the depth of cut in which ductile behavior starts, changes with crystal orientation and the directions in the crystal. Easily fractured directions disclose a critical depth of cut of 0.2 µm- 0.5 µm. On the other side, the other directions have a critical depth of cut approximately 1 µm. Tool geometry is also effective on critical depth of cut.

In the study of Hung et al.[22], the effect of crystallographic orientation in ductile regime machining of silicon wafers was investigated. Single crystalline diamond tools were used to machine the wafers at either constant depths of cuts or a taper mode to vary the depths of cut up to 1 μm. the feedrates were normalized as percentages of tool nose radii, and the machining process was performed using an ultraprecision machining system. The surface and subsurface integrity were then characterized with an atomic force microscope, a phase shit interferometer, and an ion beam system. It was reported that a ductile regime cutting was performed along the <110> directions when the maximum chip thickness of less than 0.5 μm. Machining conditions that formed thicker chips led to pitting. Surface roughness below 10 nm was measured in ductile regime machined area, but was as high as 170 nm in damaged areas. When the depth of cut was the magnitude of the tool edge sharpness, the surface finish was degraded by radial cracks in the lateral plane owing to rubbing between the tool and the workpiece.

1.6 Scope of Thesis

Optical systems with silicon material have important potential in Aselsan Inc. To manufacture silicon optics with the desired surface quality is critical to achieve high performance in imaging systems.

The surface roughness which comes out as result of turning process depends on a number of factors. The factors which are inputs of the process are cutting speed, feed, and depth of cut, tool nose radius, tool rake angle, clearance angle and cutting fluids. Rigidity of the machine, vibration, environmental factors such as, temperature, and humidity and operator are other factors.

The main scope of this study is to develop a mathematical model that lets us predict the surface roughness of mono crystal silicon substrates. The mathematical model will put the relation between the cutting parameters and the surface roughness metric Ra. Understanding the relation is of importance in achieving the best surface, or the surface that meets the minimum requirements.

In order to explore effects of parameters, a design of experiment study has to be carried out since there are lots of input parameters. Otherwise, it is practically impossible to explore all the effects simultaneously and come to a conclusion.

In this study only cutting speed, depth of cut and feed rate are selected as variable parameters. And others are all kept as constants. Besides the environmental effects are neglected even though, they have some influence on the result in ultra-precision machining process.

In Chapter 1, general information about the thermal imaging systems and the optical materials used in production of these systems have been introduced. Besides, significance of silicon among these materials has been emphasized. The previous studies about ultra precision machining of silicon has been summarized. In Chapter 2, the Single Point Diamond Turning (SPDT) technology and the tools being utilized in SPDT are presented. Furthermore, a critical issue about machining of silicon, ductile regime cutting, is described. In Chapter 3, roughness parameters and the techniques used in measurement of roughness have been given. In Chapter 4, experimental setup takes place. In this chapter, the CNC machine tool, the single crystal diamond tools used in this study and the measurement device are introduced. In Chapter 5, the results obtained in this study are presented and discussed. A mathematical model is derived in order to predict Ra value within the

defined ranges of cutting parameters. In Chapter 6, conclusions and suggested future works are presented.

CHAPTER 2

SINGLE POINT DIAMOND TURNING

2.1 Cutting Parameters in Turning Operation

The operating parameters in a turning process are the cutting speed (V), feedrate (f) and depth of cut (d). These parameters are shown on the geometry of a turning operation given in Figure 2.1.

The cutting speed is determined by the rotational speed of the spindle. Thus the cutting speed at the tool is

$$V = \pi DN \tag{2.1}$$

where N is the rotational speed of the spindle and D is the diameter of the machined surface. Therefore the average cutting speed is expressed by

$$V_{av} = \pi N \frac{D_1 + D_2}{2} \tag{2.2}$$

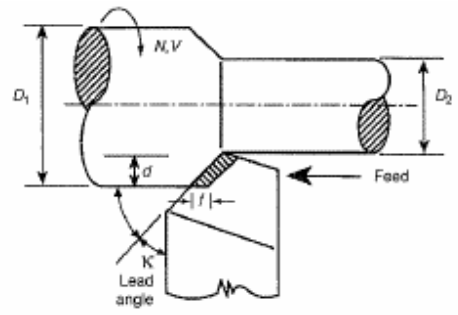

Figure 2.1 Turning Operation

The *feed (f)* is the tool advancement per revolution along its cutting path, in mm/rev. Whereas, the *feedrate (fr)* is the speed at which the tool advances into the part longitudinally, in mm/min [23]. The relation between feed and feed rate is

$$fr = fN \tag{2.3}$$

Thus, to turn a cylindrical workpiece of length l_w, the required machining time is estimated by the formula:

$$t_m = \frac{l_w}{fr} \tag{2.4}$$

The *depth of cut* determines the depth of material removed from the workpiece in a single-point cutting operation [24].

The *material removal rate* is expressed by

$$Z_w = A_c V_{av} \tag{2.5}$$

where A_c is the cross-sectional area of uncut chip and equals to

$$A_c = fd \tag{2.6}$$

2.2 Single Point Diamond Turning

Taniguchi defined ultra precision machining as "the process by which the highest possible dimensional accuracy is achieved at a given point in time" and showed the available machining techniques and the accuracy values achieved by making use of these techniques on chart which is given in Figure 2.2 [25]. Ultra precision machining is defined by Ikawa et al. as "a cutting technique which enables us to produce optical, mechanical and electronic components with micrometer or sub-micrometer form accuracy and surface roughness to within a few tens nanometer" [10].

Single Point Diamond Turning (SPDT) is a kind of ultra precision machining and by making use of SPDT submicron form accuracy and nanometer level surface finish can be attained. In the latest decades ultra precision machine tools, precise diamond tools and control technology have shown a rapid development and parallel to this advancements in the base technologies SPDT has improved. Compared with the traditional grinding and polishing methods, SPDT has some advantages. First of all, SPDT has a higher material removal rate, which results in less machining time relatively to traditional methods. SPDT is easier to be computer controlled. Therefore, automatic production is available. Furthermore, SPDT can produce highly accurate surfaces. The last but not the least, SPDT can produce not only spherical and flat surfaces but also aspheric surfaces which have a growing usage in modern optical devices [11].

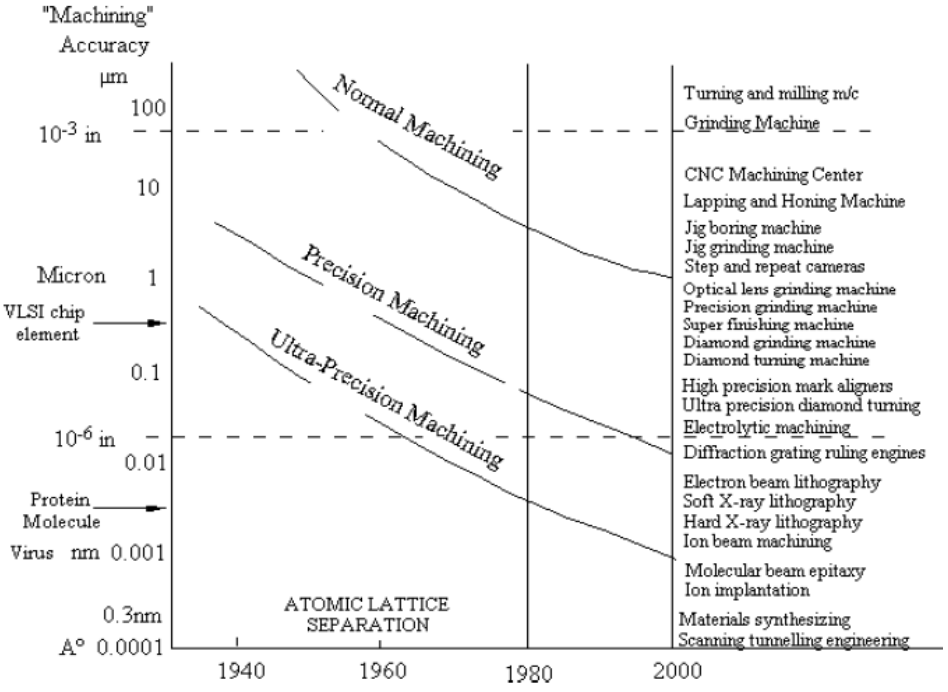

Figure 2.2 Machining Accuracies of Different Techniques [25]

2.3 Tools Used in SPDT

As it is stated in the name SPDT, single point diamond turning tools are mode of diamond crystals. Diamond is known to be the hardest of all the materials and utilized as a cutting tool where other materials cannot operate in an effective manner. Diamond tools are worn less and have a longer tool life than other tool materials such as carbides or oxides [26]. Some diamond tools are depicted in Figure 2.3.

Figure 2.3 Diamond Tools [27]

Diamonds used for tool production might be natural or synthetic. Besides, diamonds are also divided into two groups as single crystalline and polycrystalline. A view of single crystal natural diamonds is given in Figure 2.4.

Single crystal natural diamonds are commonly used for production of optical instruments and gold jewellery since production of high accuracy and finish is attainable for this tool material. Orientation of cubic structure is of important for single crystal diamond tools. Therefore the optimum orientation is selected and

diamonds are lapped according to the required shape and mounted in tool holders [26].

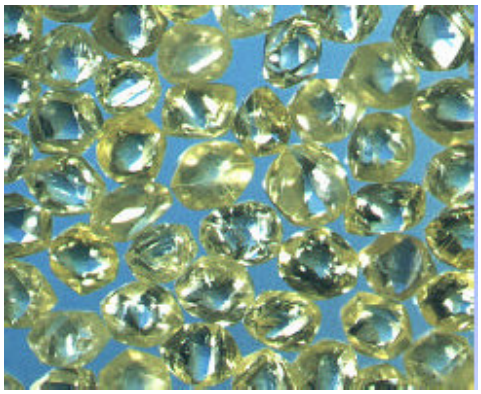

Figure 2.4 Single Crystal Natural Diamonds

Synthetic diamonds are produced by heating graphitic carbon at high temperatures above 1500° ant at ultra high pressures. By this way, small diamonds of few tenths of millimeters are obtained. Turning tools are attained by sintering of these small particles. However, it is not possible to achieve a perfect cutting as a natural diamond [26].

Single point tool geometry is defined as given in Figure 2.5. In cutting process the chip flows over the surface so called rake face. The cutting edge is formed by the intersection of the rake face with the clearance face or flank of the tool. The rake face is inclined at an angle to the axis of the bar of the work material and this angle can be adjusted to achieve optimum cutting performance for particular tool material. The nose of the tool is at the interaction of all three faces and may be sharp, but more frequently there is a nose radius between the two clearance faces.

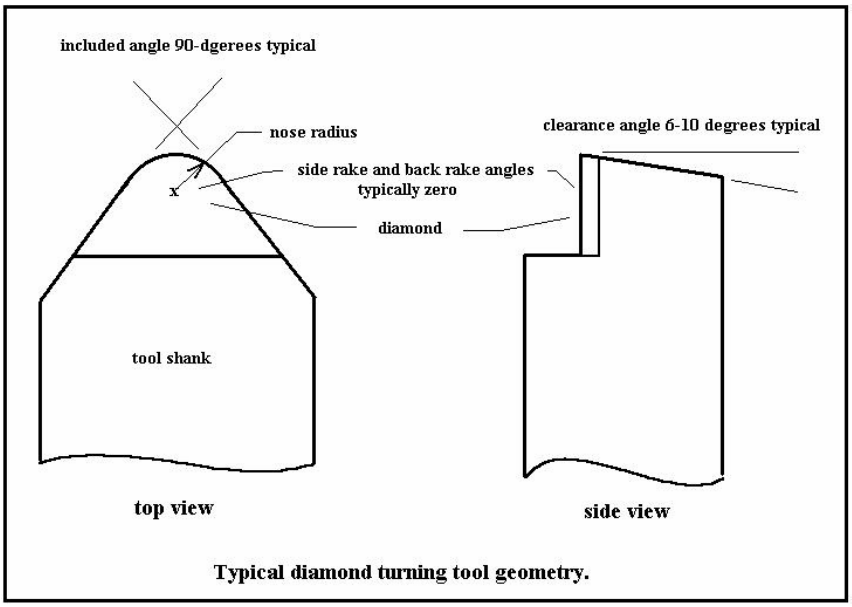

Figure 2.5 Description of Single Point Tool Geometry [28]

The diamond tools used in SPDT are grouped as “controlled waviness” and “non-controlled waviness” according to waviness control of tool radius. For the tools which are “non-waviness controlled”, the tool radius is expected to have a waviness value smaller than 1.0 µm. However, “controlled waviness” tools are guaranteed to have better waviness such as 0.75 µm, 0.50 µ, 0.25µm, 0.15µm and even 0.05 µm. Note that, decreasing waviness value of the radius, causes a rise in the prices of the tools [27]. On the other hand, by utilizing waviness controlled tools, better surface roughness values can be obtained. Figure 2.6 shows the difference between “waviness controlled” and waviness non-controlled tools”.

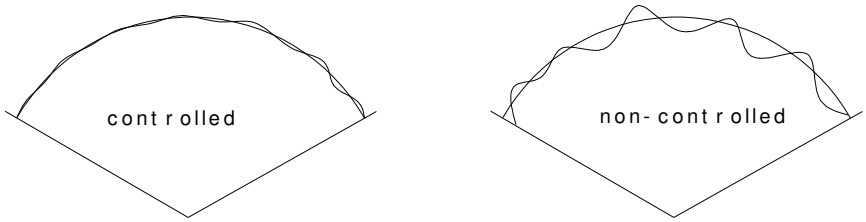

Figure 2.6 Waviness Controlled and Waviness Non-controlled Tool Radii [27]

Diamond tools with different tool radiuses from .020" to .060" are available in the market [27]. In selection of the right tool, it must be considered that, a large radius gives a better surface finish but has greater cutting forces and may distort the part. In contrast, a small radius exerts less cutting force but has more frequent turning lines within the surface finish. The difference between a large tool radius and a small tool radius is graphically represented in Figure 2.7.

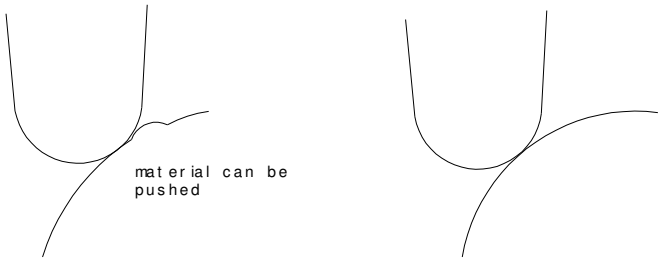

Figure 2.7 The Difference Between Large Small Tool Radii [27]

2.4 Ductile Regime Machining of Silicon

2.4.1 Brittleness vs. Ductility

Materials are classified as brittle and ductile according to their response to tensile stress before fracture. If a material can withstand extensive deformation without failing under high tensile stress, it is considered ductile. Thus, ductile fracture of a metal occurs after extensive plastic deformation. This manner of materials is called ductility. Gold, copper, aluminum, and steel express high ductility. On the other side, some materials fracture with very little plastic deformation. This called brittle fracture and the manner is named as brittleness. Glass, most ceramics, tungsten, germanium and silicon can be counted as brittle materials. [29, 30].

Toughness is measure of the amount of energy, a material can absorb before fracturing [29]. Therefore, ductile materials have higher toughness values than brittle materials. Fracture toughness is determined by the area under stress-strain curve. In Figure 2.8, stress-strain curves for ductile and brittle materials are given. It is clearly seen that, the area under the curve for a brittle material is smaller than the area of a ductile material.

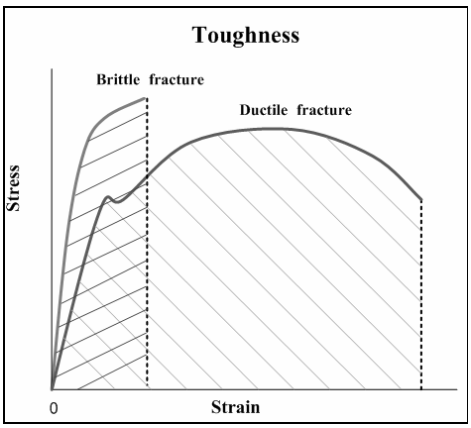

Figure 2.8 Stress-Strain Curves for Ductile and Brittle Materials

Fracture toughness values of some materials are given in Table 2.1. It is seen that, silicon has a very low fracture toughness compared with aluminum, titanium and steel.

Table 2.1 Fracture Toughness Values of Some Materials[29, 31, 32]

Material	**Fracture Toughness [MPa-m$^{1/2}$]**
Aluminum 2024-T851	26.4
Aluminum 7075-T651	24.2
Titanium Ti-6A1-4V	55
Steel 4340	60.4
17-7 pH	76.9
Soda-lime-glass	0.7-0.8
Silicon <111>	0.83-0.95

2.4.2 Ductile Regime Machining

The studies on optical quality surface machining have shown that brittle materials are to be machined in a ductile regime and this is possible under some carefully chosen machining conditions [15, 21]. The chips in the ductile regime machining are continuous. However, when ductile machining cannot be provided discontinuous chips form. Continuous chip formation produces better surfaces. Nonetheless, discontinuous chip formation produces rougher surfaces due to the fracture in chip formation zone. Continuous and discontinuous chip formations are depicted in Figure 2.9 and 2.10., respectively.

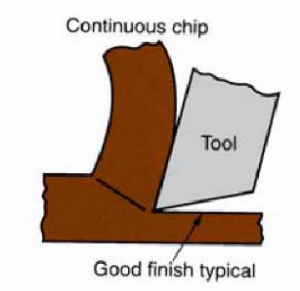

Figure 2.9 Continuous Chip Formation[33]

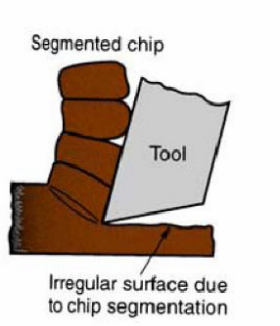

Figure 2.10 Discontinuous (Segmented) Chip Formation[33]

Ductile regime machining of a brittle material is determined by "critical chip thickness". The critical chip thickness is defined as the thickness of the chip where, the damage occurred during cutting cannot be removed by subsequent passes of the tool [34]. Material removal and chip formation in SPDT is schematically represented in Figure 2.11. When a tool passes through the material, it brings about some micro fracture damage under the surface of the material, as seen in Figure 2.12. Chip thickness *t* is the main factor influencing the stress field of cutting zone and the occurrence of microfracture. If the chip is maintained at a small value, the stress field of cutting zone will be too small to induce microfractures. So along the tool edge, there exists a critical value of chip

thickness t_c. In the region where $t > t_c$, microfractures take place in the work material during cutting. But, in the region where $t < t_c$, work material is removed by plastic deformation without fracture. This means that ductile regime machining is performed in this region. However, the location of t_c is largely depends on the tool feed. As the feed decreases, chip thickness t decreases too. Then, t_c moves upward along the tool edge. The fracture damaged region rises away from the machined plane and will be removed by the later several revolutions of the cutting tool. At the same time, the region where the work material is removed plastically is enlarged. So, given the low tool feed, smooth surface can be obtained by ductile regime machining. The cutting speed has a minimum effect on the surface finish, but a reduction of the feedrate provides an improvement of the surface finish [22].

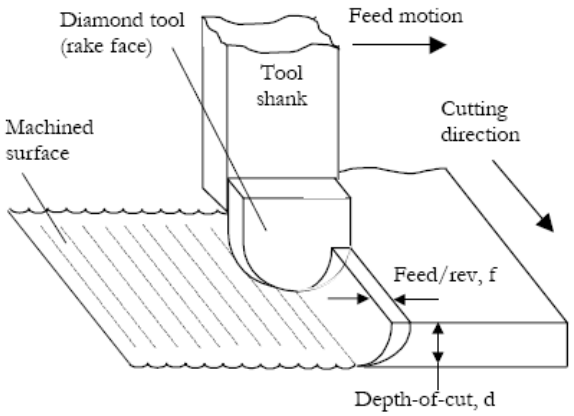

Figure 2.11 Schematic Representation of Material Removal in a SPDT [34]

The effect of depth of cut is relatively small. As it is seen in Figure 2.12, the increasing depth of cut cannot change the location of critical chip thickness. If the feedrate is large enough, ductile regime machining can be performed even under large depth of cuts. However, when the depth of cut is extremely small, no matter

how much is the feedrate, the surface quality goes seriously bad. One of the reasons is that, extremely small depth of cut significantly increases the cutting pressure between the tool edge and the workpiece. Thus, the material is in bad deforming condition of highly concentrated stress state. A lot of microfractures take place on or below the machined plane and damage the machined surface. Another reason is that, the vibration and runout of the machine tool spindle unsteadily varies the very small depth of cut. This causes a fluctuation in the deforming volume of workpiece, and sometimes even drops the cutting depth below the limiting depth of cut of the cutting tool itself. The damaged surface is formed by the serious pressing of the tool edge on the workpiece [11] .

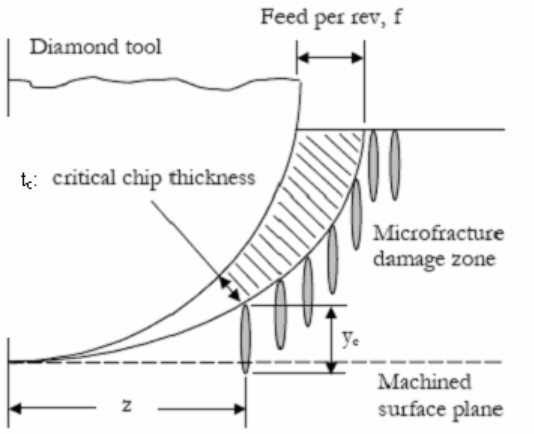

Figure 2.12 Schematic Representation of Microfracture Damage Zone Formation in a SPDT Pass [34]

A study by Leung [15] showed that, while depth of cut is increased, the thickness of the chips increases. In parallel, the average roughness value of the machined surface rises. But, when a critical value of depth of cut, and critical chip thickness

are exceeded, an extreme rise is observed in the roughness of the surface. The relation between chip thickness and roughness is given in Figure 2.13.

Rake angle of the tool affects the critical chip thickness, either [15, 20]. In Figure 2.14, it is seen that increasing negative tool rake angle, causes a rise in critical chip thickness. This condition is valid for different oriented silicon crystals.

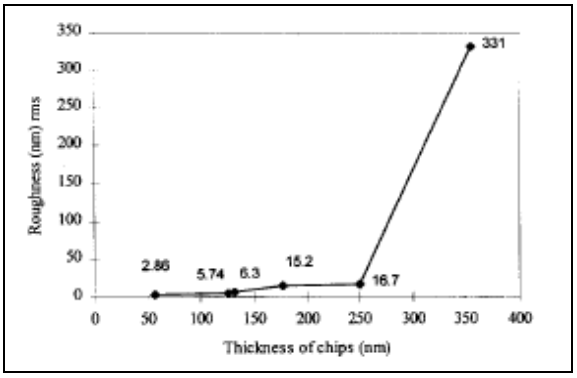

Figure 2.13 Effect of Chip Thickness on Roughness [15]

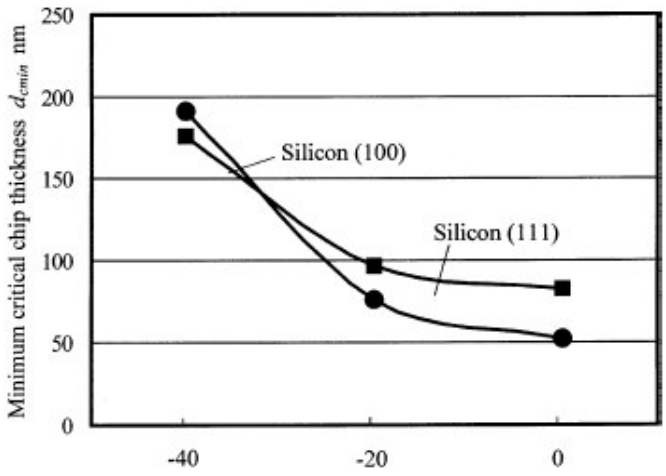

Figure 2.14 Effect of Tool Rake Angle on Critical Chip Thickness [20]

2.4.3 Effects of Crystallographic Orientation

In diamond turning of silicon some radial pitting damage zones can be observed. These zones are dependent on the cubical structure of silicon [35]. It is explained that, orientation dependent machining damages are due to the changes in tensile stress in different slip planes of silicon [36].

The crystal structure is important in understanding the damaged zones. Silicon has diamond cubic structure at room temperature (see Figure 2.15) [29]. The atoms in a silicon lattice are not isotropically distributed in space. This situation can be noticed in Figure 2.16. The anisotropy is effective on orientation dependent results, attained in machining; mechanical properties such as modulus of elasticity, hardness and fracture toughness are dependant on the directions in the lattice. [35].

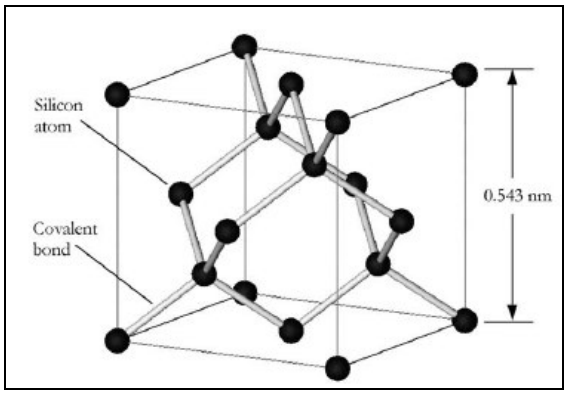

Figure 2.15 Diamond Cubic Crystal Structure of Silicon [35]

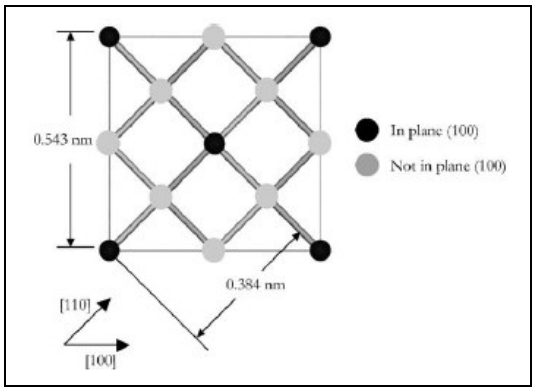

Figure 2.16 Silicon Crystal Lattice Viewed from [1 0 0] Direction [35]

Fracture toughness is also important in explaining the phenomena. Table 2.2 shows the variations in toughness values in different slip planes.

Table 2.2 Variations in Fracture Toughness in Different Slip Planes [36]

Crystal Plane	Fracture Toughness [MPam1/2]
(1 0 0)	0.95
(1 1 0)	0.90
(1 1 1)	0.82

In literature it is presented that, different surface figures can be observed, when different planes in a crystal are machined. In (1 0 0) plane damage with fourfold symmetry is remarkable, which is seen is Figure 2.17. Likewise, the schematic representation of damages which occur in slip planes (1 1 0) and (1 1 1) are given in Figures 2.18 and 2.19. Consequently, damage observed on machined surfaces of diamond cubic crystals like silicon depends on the cutting direction.

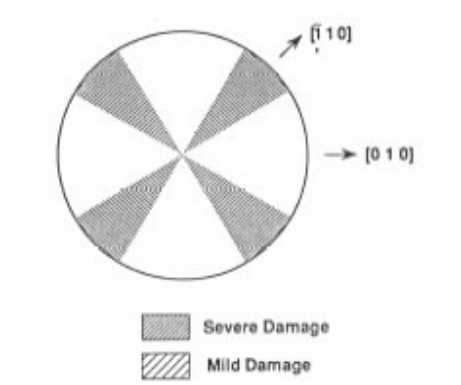

Figure 2.17 Schematic Representation of Damage in (1 0 0) Plane [36]

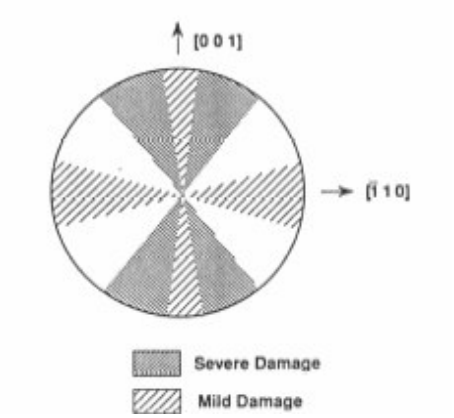

Figure 2.18 Schematic Representation of Damage in (1 1 0) Plane [36]

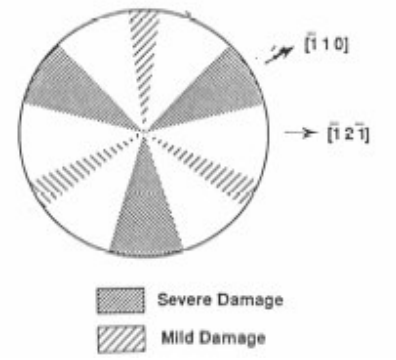

Figure 2.19 Schematic Representation of Damage in (1 1 1) Plane [36]

CHAPTER 3

SURFACE ROUGHNESS AND MEASUREMENT METHODS

3.1 Roughness Parameters

Due to the nature of machining operations, obtaining a perfect surface is not possible. There are always some unavoidable imperfections on the surface of a machined part. The surface finish of a machined part is composed of two components which are waviness and roughness [24].

Waviness refers to deviations in the surface with relatively long wavelengths or equivalently lower frequencies. Waviness may result from clamping errors, errors in the tool geometry or vibration in the machine tool [23].

On the other hand, roughness is defined as the deviation in surface profile with shorter wavelengths than those of waviness. Hence, roughness is a finer irregularity than waviness and superimposed upon waviness [24]. Roughness is dependent on feedrate, tool nose radius, tool rake angle and cutting speed. Besides, tool wear, inhomogeneities in the workpiece material, high frequency vibrations of the machining system and damage to surface caused by chip contact can also bring about roughness [23]. In Figure 3.1, waviness and roughness are depicted.

Furthermore, another characteristic of surface finish is lay. Lay is the term used to refer to the direction of the predominant tool marks, grain, or pattern of the surface roughness. All surface roughness measurements or comparisons are normally taken across the lay, as this direction gives the best comparative value [37]. Some examples to the lay types are given in Figure 3.2.

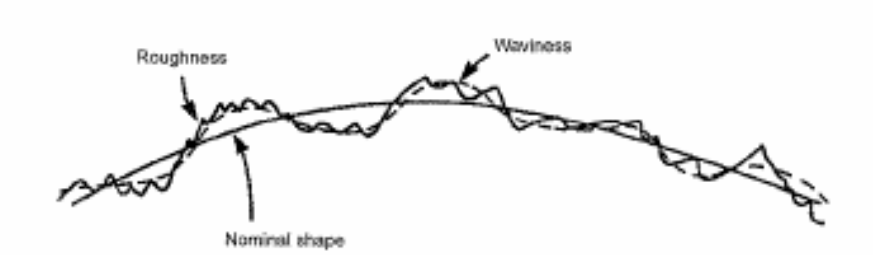

Figure 3.1 Waviness and roughness [23]

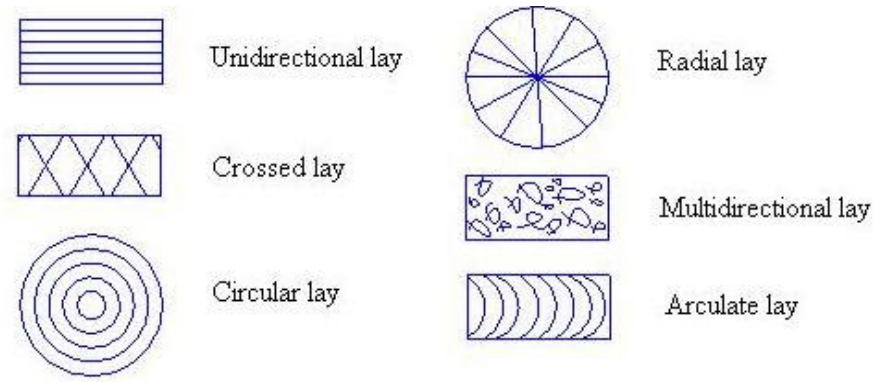

Figure 3.2 Some Lay Types [38]

Surface roughness is characterized by some parameters. These parameters are defined in national and international standards as ASME B46.1-2002, ISO 4288:1996, ISO 4287:1997 and DIN 4768:1990 [23]. Another standard is TS 971, a national standard, which covers the parameters, their values and general rules for specifying requirements at surface roughness [39]

The parameters most often used for determining the surface roughness, which are defined in the standards, are average roughness Ra, root mean square (RMS) roughness Rq, maximum peak height Rp, maximum valley depth Rv and peak-to-valley height Rt [23].

The average roughness is defined as the average absolute deviation of the workpiece from the mean line [23]. Ra is the most common roughness parameter used in practice [40]. Average roughness is given by the formula [41]

$$R_a = \frac{1}{L}\int_0^L |z(x)|dx \tag{2.1}$$

Root mean square roughness is defined as the root mean square average of the roughness profile ordinates [42]. It is formulated as [41].

$$R_q = \sqrt{\int_0^L \frac{1}{L} z^2(x)dx} \tag{2.2}$$

Average roughness and root mean square roughness are graphically represented in Figure 3.2.

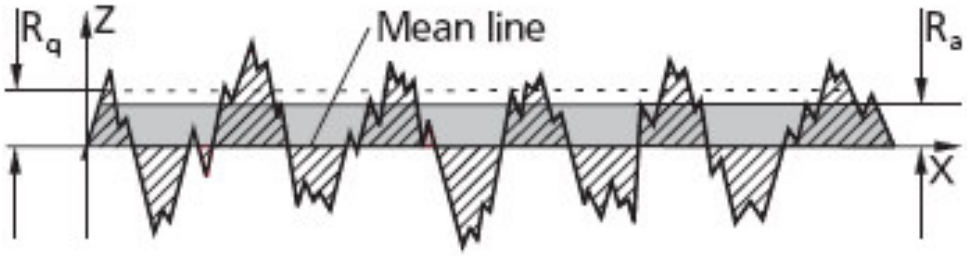

Figure 3.2 Average Roughness And Root Mean Square Roughness [42]

The maximum peak value above the mean line is Rp the maximum valley depth below mean line is Rv. These metrics are defined as follows [23], for 0<x<L

$$R_p = \max z(x) \tag{2.3}$$

$$R_v = |\min z(x)| \tag{2.4}$$

Furthermore the maximum peak-to-valley deviation is given as

$$R_t = R_p + R_v \tag{2.5}$$

3.2 Measurement of Surface Roughness

Surface roughness measurement can be attained by different measurement methods. Direct measurement method and non contact measurement technique are widely used in field. Besides, surface roughness can be measured by utilizing comparison method and on-process comparison technique [43].

3.2.1 Direct Measurement

In direct measurement technique, surface roughness is assessed by utilizing stylus probe drawn over the surface, shown in Figure 3.3. This type of instruments operate by amplifying the vertical motion as it is drawn across the surface [24]. The displacement of the stylus is converted into electrical signals which can be analog or digital [38]. Afterwards, electrical signals are processed and required data is obtained.

Cut-off length is an important consideration for an accurate measurement. Cut-off length determines which part of the profile belongs to waviness. If the undulations have much larger wavelength than our examination length this means that our sample will include very little undulation but it concentrates on roughness. Maximum wavelength considered is known as cut-off length [40]. Cut-off length is standardized in ISO, TSE at 0.08 mm, 0.25 mm, 0.80 mm, 2.50 mm, 8.00 mm,

and 25.00 mm that is selected depending on the surface being explored. Cut-of length and other significant lengths are shown in Figure 3.4.

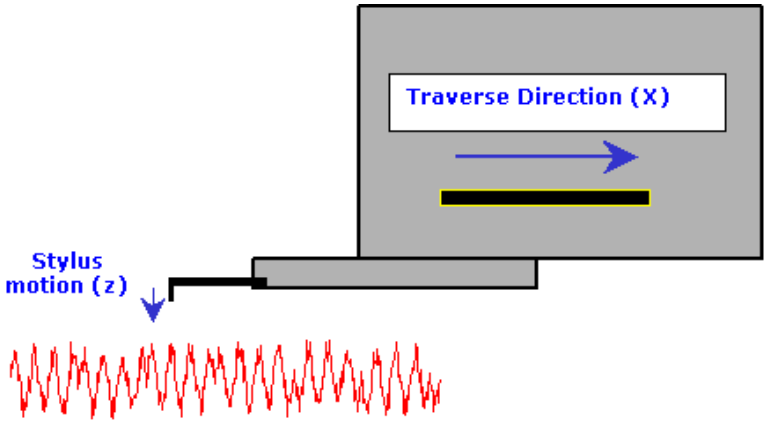

Figure 3.3 Stylus Probe Instrumentation [44]

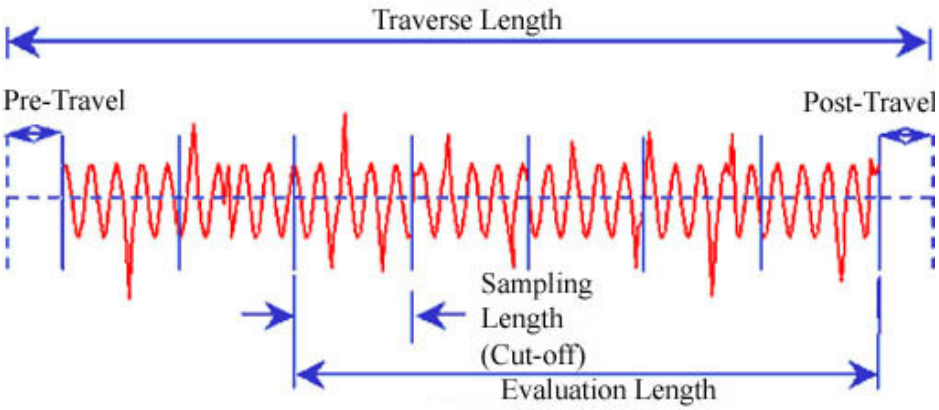

Figure 3.4 Significant lengths in roughness measurement [44]

What is more, sampling length is also of importance for a roughness measurement. Samples are taken by dividing the surface data into equal sample lengths as shown

in Figure 3.4. The sample length is equal to the cut-off length. Namely, data is divided into pieces of cut-off length. In most cases five samples are used for roughness analysis [44]. The five consequent sampling lengths make up evaluation length [42].

Additionally, that total length that the stylus moves is called traverse length. The first part of traverse length is named as pre-travel and the last part is post-travel length [42]. These are shown in Figure 3.4. Pre-travel and post travel lengths are evaluated in filtering the data.

3.2.2 Non-Contact Measurement

Non-contact measurement techniques depend on optical instrumentation. This kind of instruments is divided into two main groups, such as profilers and interferometers. Profilers are utilized to measure waviness on the specimen. However interferometers are the equipments that measures roughness of the surfaces. Interferometers are commonly named as “white light interferometers”.

When light is incident on a rough surface a proportion of it, depending on the local physical properties of the surface, is reflected. The reflected beam carries information about the roughness of the surface [45]. White light interferometry works on this principle. In this technique, the intensity of interfering light is used to determine the topology of a surface.

In white light interferometry, a light beam passes through an interferometric objective containing a beam splitter that reflects half of the incident beam to a reference surface and passes half of the test surface. Light reflected from the test and reference surfaces recombines and interferes, forming a pattern of dark and light bands, or fringes, called an interferogram. The objective is translated, altering

the optical path difference between the test and reference surfaces. As it translates, several interferograms are sequentially imaged, and height data are calculated from the interference data. Working principles of white light interferometry is schematically represented in Figure 3.5. Interferometers can measure 0.1 nm Ra roughness values [40].

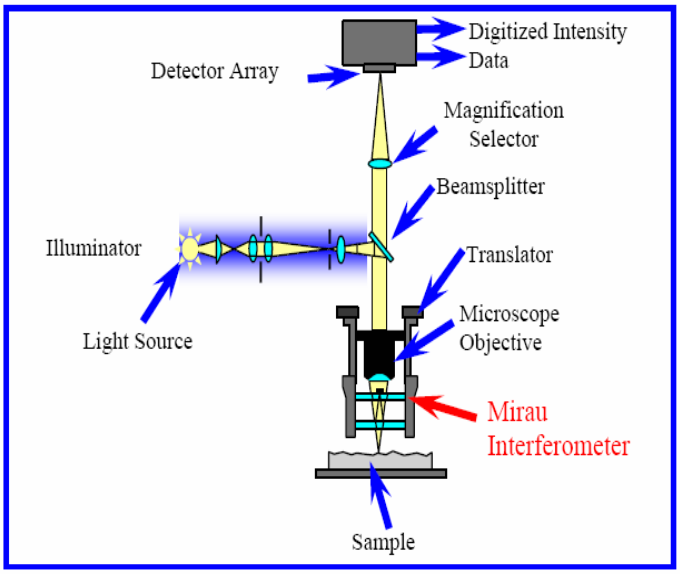

Figure 3.5 White Light Interferometer [46]

Modern interferometers are sophisticated devices working on a computer program which translated interferograms into images on the screen. Once the data is taken, the program calculates all the roughness parameters and presents an oblique and a solid plot of the measured are. A sample outpour screen is given in Figure 3.6.

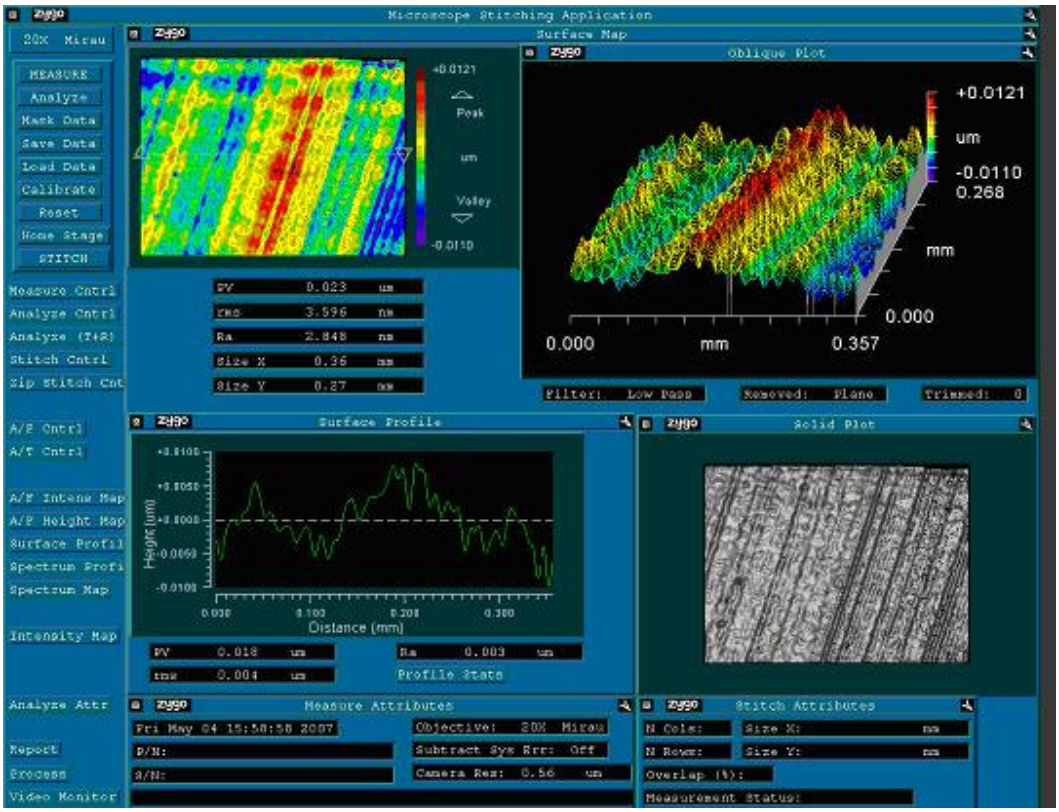

Figure 3.6 A output screen with white light interferometer

3.2.3 Other Methods

Besides the methods mentioned above, there exist some others which are utilized in order to evaluate the surface roughness of a specimen. “Comparison techniques” use specimens of surface roughness produced by the same process, material and machining parameters as the surface to be compared. Visual and tactile senses are used to compare a specimen with a surface of known surface finish. [43]. Furthermore, “machine vision” is employed for measuring roughness. A light source illuminates the surface and the view of the surface is sent to a computer to be analyzed in digital format. The digitized data is evaluated with a correlation chart, and actual roughness value is figured out [43]. “Acoustic radiation” interacts

with rough surfaces in a similar way with light. Therefore sound is also used to measure surface roughness [45].

3.3 Filtering

In roughness measurement, waviness is separated from the result by employing some filters. These filters might be applied in graphical, electrical, mechanical, or digital means [37].

Graphical filtering is applied by decomposing the profile into a number of consequent equal sample lengths. Here, sample length should be shorter than the wavelength of the waviness of surface profile (see Figure 3.7). To each sample length, a separate straight mean line is fitted, by least squares or an equivalent method, and then all the mean lines are joined in a single straight line shown in Figure 3.8. [45]. However, if the sample wavelength is larger than wavelength than the filters data will contain waviness information in the output which is depicted in Figure 3.9

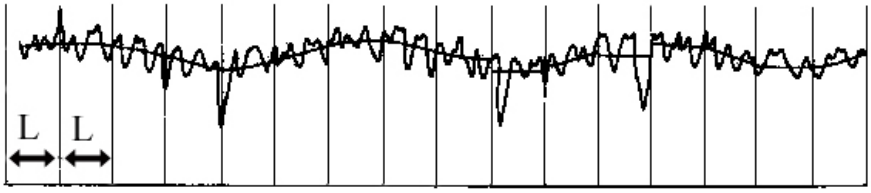

Figure 3.7 Sample length smaller than wavelength [45]

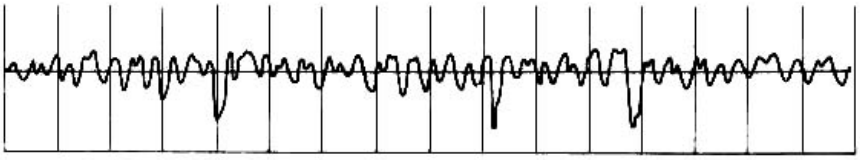

Figure 3.8 Redrawing of Figure 3.6 after filtering [45]

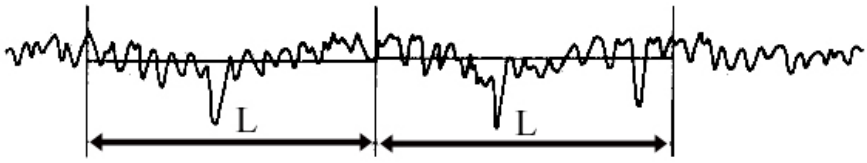

Figure 3.9 Sample length is larger than wavelength [45]

Electrical filtering can be attained by a resistor-capacitor (RC) circuit. A sample RC circuit is shown in Figure 3.10. The aim is to apply a high-pass filter to eliminate waviness and to separate roughness data from the profile [45]. A similar circuit might be utilized in order to filter high frequency data and observe waviness of the surface. A surface profile filtered by electrical means is given in Figure 3.11.

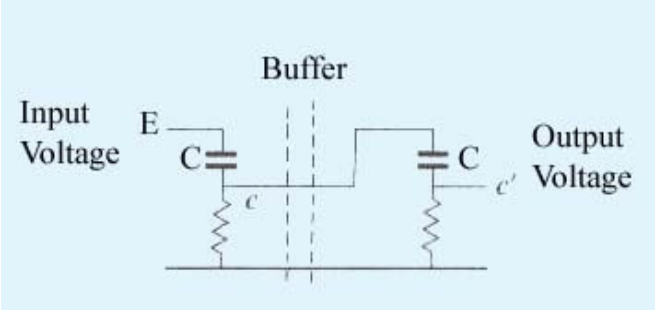

Figure 3.10 RC Filter [41]

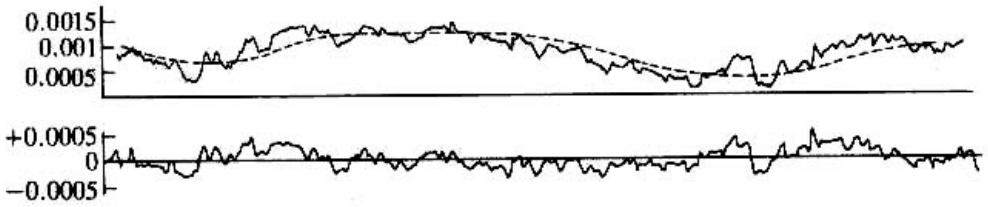

Figure 3.11 Electrically filtered data [41]

Mechanical filtering is performed by using a skid sliding over the surface and establishing a reference line for measurement. In Figure 3.12, a mechanical filter is shown. The skid is recommended to be at least 50 times larger than the stylus. Since the radius of the skid is larger than the spacing of the peaks, the movement line is almost straight and up and down movements of the skid is insignificant. The rounded skid tends to follow the undulation therefore widely spaced undulations are eliminated [41].

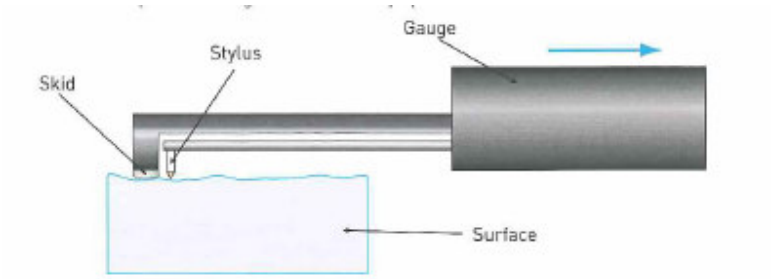

Figure 3.12 Mechanical filtered roughness measurement [47]

Computerized surface measurement instruments such as, interferometers or some digital stylus probe instruments, digitizes collected surface data and store it in the computer memory. This data is filtered computationally. This process is named as

“digital filtering” The advantage of this approach is that the same raw data can be filtered multiple times with different cut-offs or different filtering algorithms to compare the results [38].

CHAPTER 4

EXPERIMENTAL SETUP FOR SILICON MACHINING

4.1 Machining Setup

In this experimental study, machining operations are held by utilizing single point diamond turning (SPDT) machine, Nanoform 350 [48], shown in Figure 4.1. Features of the machine are given in Appendix A. Besides, the part code program run in the operations is provided in Appendix B.

As seen in Figure 4.2, a vacuum chuck is used and the work piece is held by the chuck without applying any force at the peripheral of the workpiece, which is a crucial point in manufacturing of lenses.

In general diamond turning operations, the work is held by a rotating spindle and the cutting tool is fed into the workpiece. Unlike conventional lathe, Nanoform 350 has the workpiece holding spindle mounted on the X axis, perpendicular to the cutting tool on Z axis. Both X and Z axis slides move under computer control, allowing the generation of any surface of revolution that can be described mathematically. Coordinated simultaneous movement of the axes allows precision manufacture of spheres, aspheres, hyperbolas, parabolas and other precision components. On the other hand, due to being a 2-axis CNC machine, the machine tool cannot perform operations with constant cutting speed and feed, at the same time. If constant tool advancement in radial direction per revolution is required, then the operation must be performed with constant spindle speed.

To align the axis of the workpiece and the spindle axis is defined as “centering”. Centering the workpiece is rather significant in turning. For this aim, a dial indicator is used. The dial indicator is coupled with the controller computer of the

lathe. The stylus of the indicator is touched on the lateral surface of the workpiece as it is shown in Figure 4.4, and the dial indicator is set to zero. Then, the chuck is slowly rotated by hand. If the reading on the screen (Figure 4.4-b) deviates, this is interpreted as the workpiece is not in the center. Thus, the workpiece is moved to the center by gentle hits with an appropriate tool such as a plastic hammer. The position is checked again and the workpiece is repositioned, if it is necessary. This procedure has to be performed for every workpiece mounted on the chuck.

Figure 4.1 A view of Nanoform 350 – Ultra precision machining system [48]

In machining operations, N020TG and N020WG type turning tools of Contour Fine Tooling Company are employed. The detailed information on nomenclature of the tool types and properties of the tools are given in Appendix C. Nevertheless, N020TG describes a tool whose radius waviness in non-controlled. The tool has a nose radius is 0.50 mm, rake angle of -15°,and clearance angle of 10°. In addition, in N020WG the difference is rake angle which is -25°. Further information about tools and tool geometries is available in Chapter 2. Moreover, on other component

of machining is cutting fluids. In this study, Clairsol 330 is used as a cutting fluid. Properties of Clairsol 330 can be found in Appendix D.

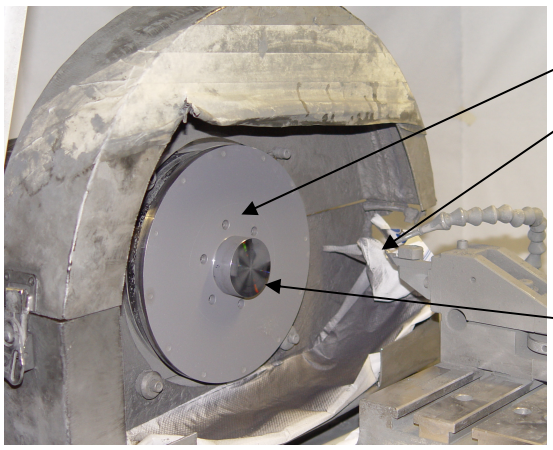

Figure 4.2 Machining Setup

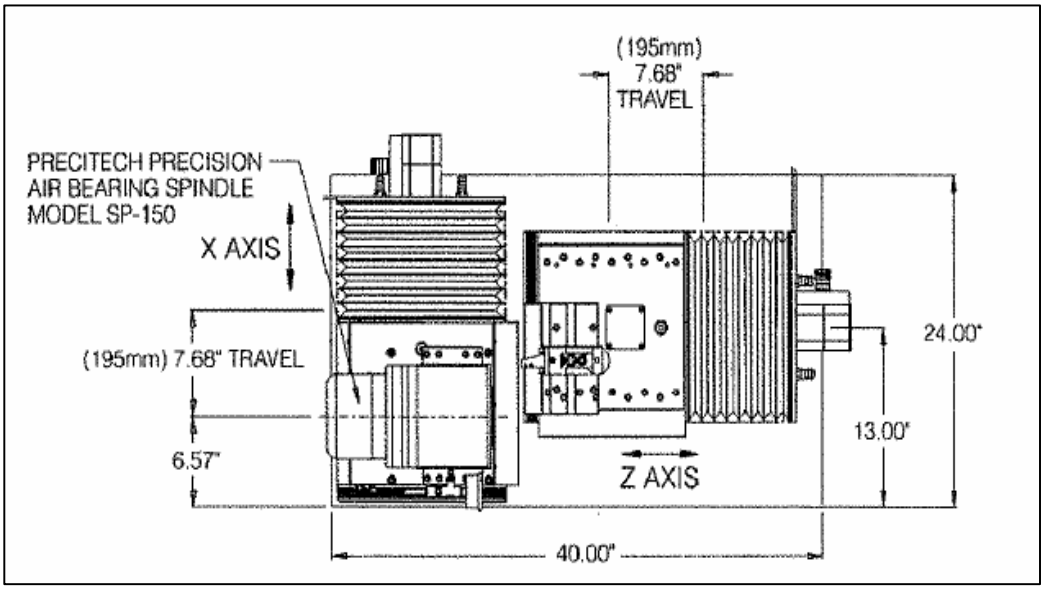

Figure 4.3 Schematic Representation of Nanoform 350 [49]

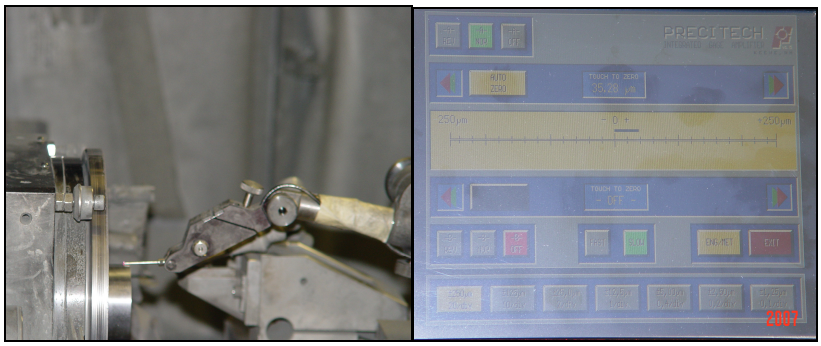

(a) **(b)**

Figure 4.4 Centering the Workpiece with a Dial Indicator

4.2 Surface Roughness Measurement

The surface roughness of machined silicon substrates is measured by using Zygo Niewview 5000, shown in Figure 4.5, which is a non-contact, scanning white-light and optical phase shifting interferometer [50]. White light interferometry is powerful method to measure surface roughness values accurately. Vertical resolution of New View 5000 is 0.1 nm. Specifications of New View 5000 are given in Appendix E. Principles of white light interferometry has been introduced in Chapter 3. A sample measurement has been given in Figure 3.6.

Figure 4.5 Zygo New View 5000 White Light Interferometer [50]

4.3 Design of Experiment

In a machining process, there exist several factors affecting the result. Exploring all the factors would require huge number of experiments, which is impractical. In turning process; the factors affecting the surface finish can be counted as: cutting speed, feedrate, depth of cut, tool nose radius, tool rake angle, clearance angle and cutting fluids. Moreover, environmental factors such as temperature, humidity may be effective on the result. Besides, the machine tool itself is a factor on the result, either. Consequently, the experimentation strategy must be designed according to the requirements, constraints such as, time, cost and precision.

"One factor at a time strategy" is a common engineering practice. In this method, a starting point and a range for each factor is selected. Then each factor is applied in different values while other factors kept constant at their starting point values to find out the effect of that factor in the process. However, the "one factor at a time strategy" is not considering the interactions between the factors and their effect on the process when they are changed together. As the one factor at a time strategy fails to consider any possible interaction between the factors, it may give poor results. Therefore, the factorial experiment method is used which also consider the interaction effects [51].

A full factorial design contains the complete matrix of every possible experiment. The full factorial design requires many experimental runs. Although the results from a full factorial design look like more comprehensive, the full set of experiments is rarely necessary, especially for a screening experiment and takes a long time. Therefore, it is often not economical and practical.[52].

In general, factorial designs are the most efficient experimental method for the types of experiments when there is an interaction between the factors. By a

factorial design it is meant that in each run of the designed experiment, all possible combinations of the levels (values) of the factors (parameters) are investigated [53]. The factorial design provides the result by limiting the number of experiments and it saves time and effort compared to full factorial design.

In this experimental study, only the cutting parameters; cutting speed, feedrate and depth of cut are taken into account. The other parameters are kept as constants in the experiments. The experimentation strategy is selected as 2^3 factorial method, since affects of only cutting parameters are investigated. Information about 2^3 factorial method is given in Appendix F. The selected values for experiments are given in Chapter 5.

CHAPTER 5

DISCUSSION OF EXPERIMENTAL RESULTS

During the study, silicon specimens were machined under different cutting conditions. The experiments were conducted with three groups. In the first group of experiments, the spindle speed was kept constant during machining. In the second and the third groups, the cutting speed was constant; however the tools with different rake angles were used. The experiment groups and discussion of the obtained results are given in the following sections. The results are evaluated by comparing the results with the optical requirements specified in the technical documents of Aselsan Inc. In these documents, the roughness criterion is given as the maximum value for the average roughness equals to 1 μ" (25 nm) [54].

5.1 First Set of Experiments

In the experiments, the cutting fluid was selected as Clairsol 330, on which additional information is given in Appendix D. The tool was N020TG of Contour Fine Tooling Company. A tool with a rake angle of -15° was used. The clearance angle of the tool was 10°. The cutting fluid properties and the tool parameters are given in Table 5.1.

In this set, the experiments were conducted with constant spindle speed. For rough cut, all the specimens were cut with a spindle speed of 2000 rpm, a depth of cut of 5μm and a feedrate of 5 mm/min. These values are recommended by the machine tool manufacturer [27]. This operation was carried out in order to standardize the surfaces of all the specimens, before the finish cut. For finish cut, an upper and a lower value were selected for each cutting parameters. The selected lower and the upper values of parameters were 1000 rpm and 3000 rpm for spindle speed; 2 μm

and 5 µm for depth of cut and 1 mm/min and 3 mm/min for feedrate. Consequently, regarding "2^3 factorial design approach", each combination of cutting parameters formed a corner of the rectangular prism shown in Appendix G. The selected cutting parameters are given in Table 5.2.

Table 5.1 Cutting Fluid and Tool Parameters

Cutting Fluid	Clairsol 330
Tool	N020TG
Tool Radius	0.50 mm
Tool Rake Angle	-15°
Tool Clearance Angle	10°

Table 5.2 Cutting Parameters for Set 1

Experiment Number	Spindle Speed [rpm]	Depth of Cut [µm]	Feedrate [mm/min]
1	1000	2	1
2	3000	2	1
3	1000	5	1
4	3000	5	1
5	1000	2	3
6	3000	2	3
7	1000	5	3
8	3000	5	3

Cutting speed, depth of cut and feedrate have influence on roughness [33]. Thus, the roughness values deviate in radial direction, in constant spindle speed facing operation. Considering this situation, the measurement points were selected at different distances as 4 mm, 8 mm, 12 mm, 16 mm and 20 mm from the center of the workpiece, as shown in Figure 5.1. The measured Ra values are presented in Table 5.3. In the table specimen number is designated as "Spec. #" and the

measurement point number on that specimen is named as “Meas’t #”. Measurement radius refers with the distance of the measurement point form the center of the specimen. Cutting speed is calculated for each measurement point. The relation between the cutting speed and the spindle speed has been given in Equation 2.1.

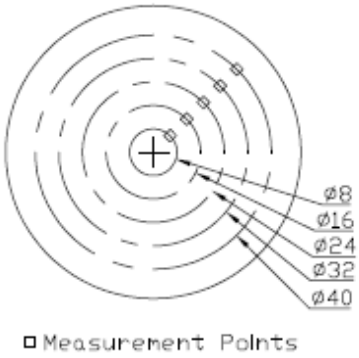

Figure 5.1 Surface Roughness Measurement Points in Set 1

Figure 5.2 graphically shows the changes of Ra for the spindle speeds N=1000 rpm and N=3000 rpm. In this experiment, the depth of cut was 2 µm and the feedrate was selected as 1 mm/min. It is clearly seen that, N=3000 rpm provides a better surface finish than N=1000 rpm. This observation is supported by the other plots in Figures 5.3- 5.5. Further discussion is available in Section 5.4.

In Figure 5.3, a depth of cut of 2 µm and a feedrate of 3 mm/min were utilized. This case is very similar with the one, discussed above. Increasing the feedrate slightly raised the Ra values for N=3000 rpm. On the other hand, for N=1000, Ra shows dramatic rise and a drop down is observed with increasing cutting speed.

Table 5.3 Ra Values Measured in Set 1

Spec. #	Meas. #	Meas't. Radius [mm]	N [rpm]	V [m/min]	d [µm]	fr [mm/min]	Ra [nm]
1	1	4	1000	12,57	2	1	6,0
1	2	8	1000	25,13	2	1	3,9
1	3	12	1000	37,70	2	1	4,5
1	4	16	1000	50,27	2	1	5,1
1	5	20	1000	62,83	2	1	4,9
2	1	4	1000	12,57	2	3	29,3
2	2	8	1000	25,13	2	3	27,7
2	3	12	1000	37,70	2	3	21,2
2	4	16	1000	50,27	2	3	20,1
2	5	20	1000	62,83	2	3	13,0
3	1	4	1000	12,57	5	1	14,5
3	2	8	1000	25,13	5	1	11,6
3	3	12	1000	37,70	5	1	12,3
3	4	16	1000	50,27	5	1	10,0
3	5	20	1000	62,83	5	1	14,8
4	1	4	1000	12,57	5	3	14,5
4	2	8	1000	25,13	5	3	14,3
4	3	12	1000	37,70	5	3	10,3
4	4	16	1000	50,27	5	3	9,4
4	5	20	1000	62,83	5	3	10,1
5	1	4	3000	37,70	2	1	2,3
5	2	8	3000	75,40	2	1	2,5
5	3	12	3000	113,10	2	1	2,0
5	4	16	3000	150,80	2	1	2,2
5	5	20	3000	188,50	2	1	2,3
6	1	4	3000	37,70	2	3	3,2
6	2	8	3000	75,40	2	3	1,8
6	3	12	3000	113,10	2	3	3,0
6	4	16	3000	150,80	2	3	1,7
6	5	20	3000	188,50	2	3	1,7
7	1	4	3000	37,70	5	1	2,3
7	2	8	3000	75,40	5	1	8,0
7	3	12	3000	113,10	5	1	9,5
7	4	16	3000	150,80	5	1	5,7
7	5	20	3000	188,50	5	1	2,8
8	1	4	3000	37,70	5	3	2,0
8	2	8	3000	75,40	5	3	2,1
8	3	12	3000	113,10	5	3	1,4
8	4	16	3000	150,80	5	3	1,4
8	5	20	3000	188,50	5	3	1,7

In Figure 5.4, the depth of cut is 5 µm and the feedrate is 1 mm/min. Again N=3000 rpm provides a better surface than N=1000 rpm. Although, both curves do not represent a meaningful trend, 3000 rpm presents better surface quality than 1000 rpm.

In Figure 5.5 a depth of cut of 5 µm and a feedrate of 3 mm/min were used. N=3000 rpm spindle speed gives a better surface than N=1000 rpm, which is parallel with the previous results. Besides, the Ra roughness for N=3000 rpm is about 2 nm.

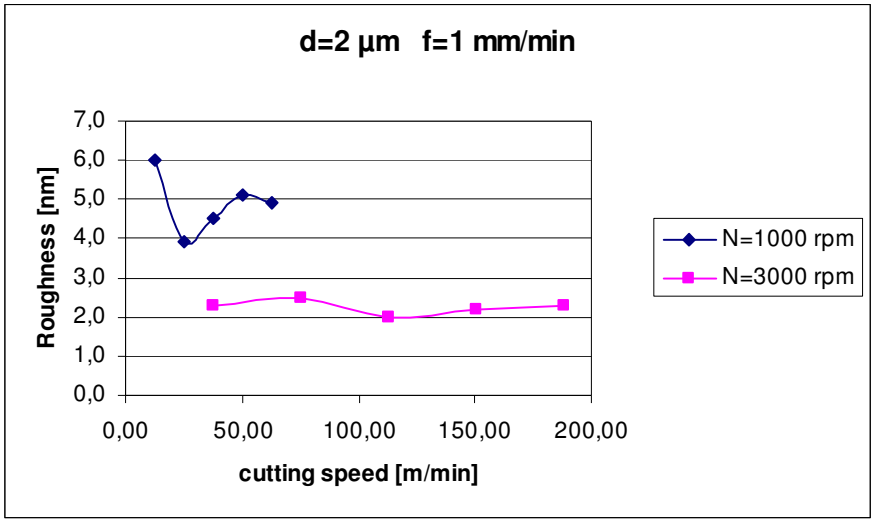

Figure 5.2 Cutting Speed vs. Roughness (d=2 µm, fr=1 mm/min)

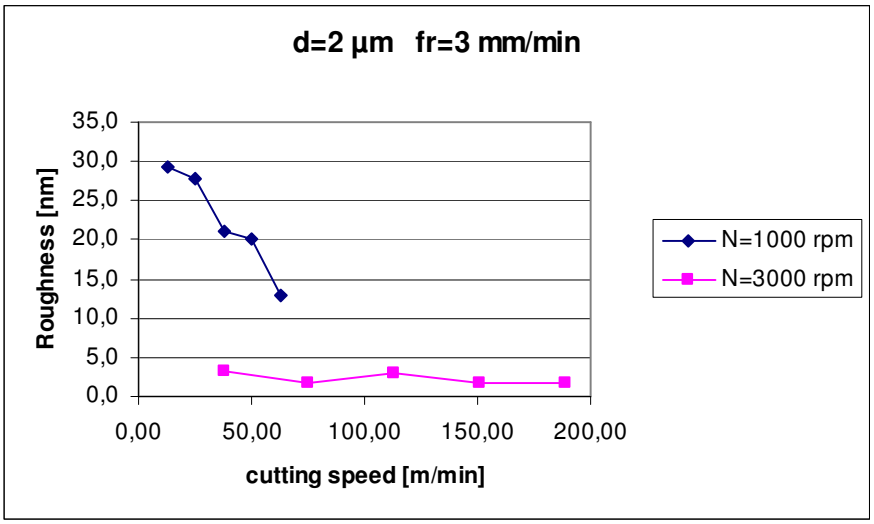

Figure 5.3 Cutting Speed vs. Roughness (d=2 µm, fr=3 mm/min)

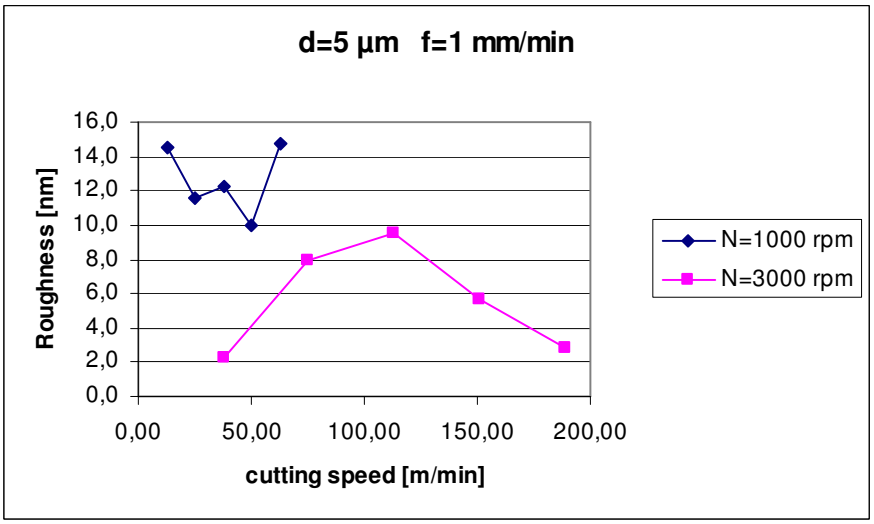

Figure 5.4 Cutting Speed vs. Roughness (d=5 µm, fr=1 mm/min)

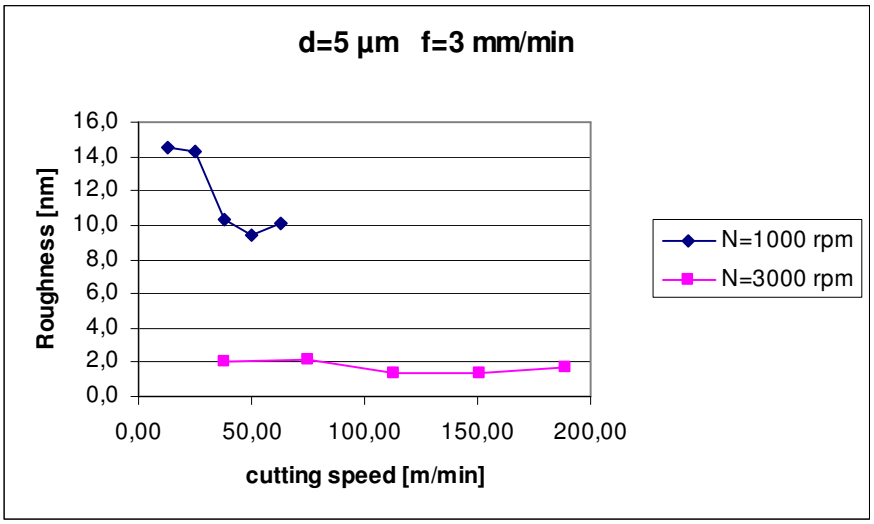

Figure 5.5 Cutting Speed vs. Roughness (d=5 µm, fr=3 mm/min)

5.2 Second Set of Experiments

In the second set of experiments the same cutting fluid and tool with the first set were used. The cutting fluid and tool parameters have been given in Table 5.1. This set of experiments was conducted with constant cutting speed. The upper and lower values for cutting speed were selected as 50 m/min and 150 m/min. In addition, the maximum spindle speed was set to 3500 rpm. The spindle speed goes to infinity as the tool approaches to the center of the workpiece in constant cutting speed face turning operations. The relation between spindle speed and cutting speed has already been given in Equation 2.1. In the first set of experiments, the upper and the lower values of cutting parameters had been selected too close to each other. Therefore, in the second set of experiments, the upper and the lower values of cutting parameters are changed as 1 µm and 10 µm for depth of cut and, 1 mm/min and 10 mm/min for feedrate, in order to observe within a wider range. Table 5.4 - 5.6 present the cutting conditions and the measured Ra values in three repeated experiment groups.

Furthermore, in this set, three areas were defined on the surface of the specimens. The outer region is the annulus between ø50 and ø30 diameters. The second region is bounded by ø30 and ø10 diameters. The third one is the inner region of ø10 circle. In the first and the second regions three arbitrary measurement points were selected as shown in Figure 5.6. No measurements were taken in the inner circle, because constant cutting speed was not achievable inthere.

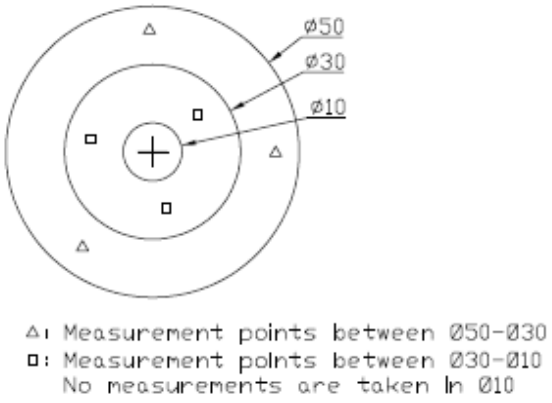

Figure 5.6 Surface Roughness Measurement Points in Set 2-3

The first two replicates were cut with the same tool, which had been also used in the first set of experiments. Regarding the unrepeatable results, the tool was changed with a new one to avoid the effect of worn tool. Nevertheless, the results did not differ as shown in Table 5.6. The comparison of three replicates is given in Table 5.7. It is clearly seen that, totally different Ra values can be obtained with the same cutting conditions. Even using the same cutting parameters very different surface textures have been observed as in Figure 5.7 and 5.8.

Table 5.4 Cutting Parameters and Measured Ra Values in 2nd Set–Replicate 1

Exp. Num.	V [m/min]	d [µm]	fr [mm/min]	Ra [nm] Msr.1	Ra [nm] Msr.2	Ra nm] Msr.3	Ra [nm] Avg.
1	50	1	1	0.4	1.0	0.7	0.7
2	150	1	1	6.5	7.8	10.6	8.3
3	50	10	1	3.8	2.2	4.0	3.3
4	150	10	1	16.1	14.5	7.7	12.8
5	50	1	10	3.4	10.4	15.2	9.7
6	150	1	10	12.4	4.6	5.3	7.4
7	50	10	10	2.5	8.4	12.4	7.8
8	150	10	10	13.0	6.2	5.2	8.1

Table 5.5 Cutting Parameters and Measured Ra Values in 2nd Set–Replicate 2

Exp. Num.	V [m/min]	d [µm]	fr [mm/min]	Ra [nm] Msr.1	Ra [nm] Msr.2	Ra [nm] Msr.3	Ra [nm] Avg.
1	50	1	1	2.9	1.9	3.3	2.7
2	150	1	1	24.3	18.8	26.4	23.2
3	50	10	1	2.2	1.9	7.3	3.8
4	150	10	1	16.7	9.5	5.2	10.4
5	50	1	10	2.4	4.1	8.9	5.1
6	150	1	10	7.8	5.8	10.3	8.0
7	50	10	10	5.9	4.1	2.8	4.3
8	150	10	10	9.9	7.2	6.4	7.8

Table 5.6 Cutting Parameters and Measured Ra Values in 2nd Set–Replicate 3

Exp. Num.	V [m/min]	d [µm]	fr [mm/min]	Ra [nm] Msr.1	Ra [nm] Msr.2	Ra [nm] Msr.3	Ra [nm] Avg.
1	50	1	1	0.7	1.8	1.5	1.3
2	150	1	1	8.6	21.6	19.4	16.5
3	50	10	1	1.9	3.1	3.6	2.8
4	150	10	1	1.7	1.6	1.3	1.5
5	50	1	10	1.0	0.4	0.9	0.8
6	150	1	10	14.9	10.3	9.6	11.6
7	50	10	10	23.7	26.1	28.6	26.1
8	150	10	10	15.6	17.2	16.9	16.6

Table 5.7 Comparison of Replicates 1-2-3

Exp. Num.	V [m/min]	d [µm]	fr [mm/min]	Ra Average Replicate 1	Ra Average Replicate 2	Ra Average Replicate 3
1	50	1	1	0.7	2.7	1.3
2	150	1	1	8.3	23.2	16.5
3	50	10	1	3.3	3.8	2.8
4	150	10	1	12.8	10.4	1.5
5	50	1	10	9.7	5.1	0.8
6	150	1	10	7.4	8.0	11.6
7	50	10	10	7.8	4.3	26.1
8	150	10	10	8.1	7.8	16.6

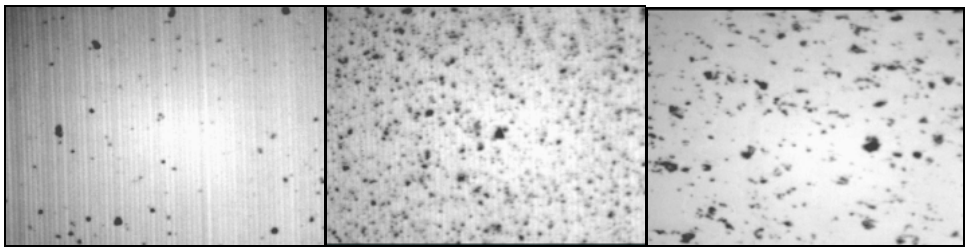

a) Ra=1.0 nm **b) Ra=2.9 nm** **c) Ra=1.5 nm**

Figure 5.7 Views from Surfaces Face Turned with Cutting Parameters: V= 50 m/min, d= 1µm, fr= 1 mm/min

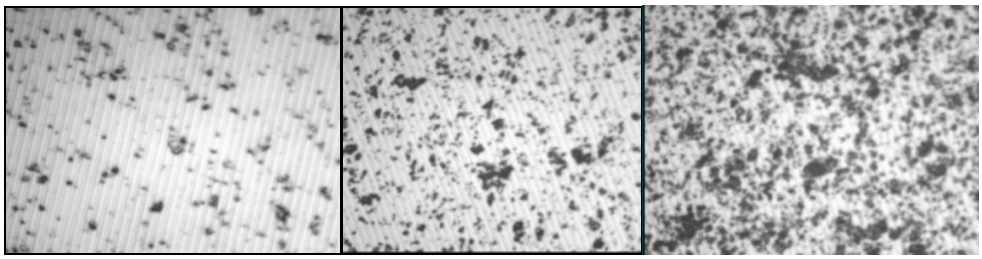

a) Ra=13.0 nm **b) Ra=6.4 nm** **c) Ra=17.2 nm**

Figure 5.8 Views from Surfaces Face Turned with Cutting Parameters: V=150 m/min, d=10µm, fr=10 mm/min

In this set of experiments, it has also been observed that some patterns of cloudy regions occur as described in Chapter 2. The patterns are shown in Figure 5.9-5.12.

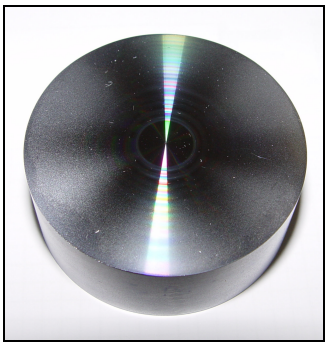

Inner Annulus V=50 m/min, d=1µm, fr=1 mm/min
Outer Annulus V=150 m/min, d=1µm, fr=1 mm/min

Figure 5.9 A View of Cloudy Region Formation with Num: 1-2

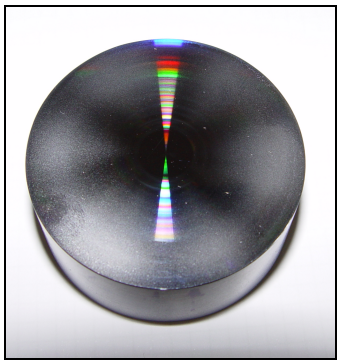

Inner annulus V=50 m/min, d=10µm, fr=1 mm/min
Outer Annulus V=50 m/min, d=10µm, fr=1 mm/min

Figure 5.10 A View of Cloudy Region Formation Exp. Num: 3-4

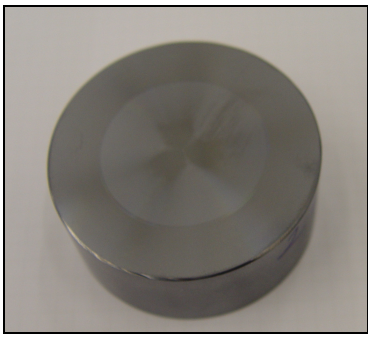

Inner annulus V=50 m/min, d=10 µm, f=1 mm/min
Outer Annulus V=150 m/min, d=10 µm, f=1 mm/min

Figure 5.11 A View of Cloudy Region Formation Exp. Num: 5-6

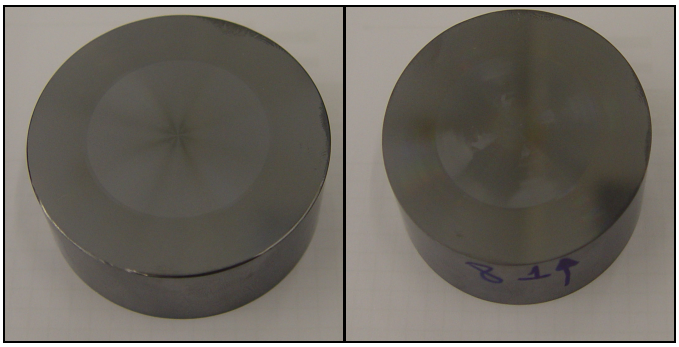

Inner annulus V=50 m/min, d=10 µm, f=10 mm/min
Outer Annulus V=50 m/min, d=10 µm, f=10 mm/min

Figure 5.12 Cloudy Region Formation with Exp. Num: 7-8

As previously discussed in Chapter 2, Blackley [36] stated that, these patterns occur depending on crystal orientation of the silicon and cutting parameters. Besides Blackley, the patterns were also reported by Leung [15], Chao [21] and O'Conner [35]. It was mentioned that, the cloudy regions are dependent on orientation. Different orientations of silicon crystals present different patterns. The

figures observed in this set of experiments, which ara given in Figure 5.9-5.12, have different number of cloudy zone arms as shown in Figures 2.17, 2.18 and 2.19. Therefore, it is understood that, the silicon specimens used in this study have different orientations.

The results presented above could not be used to build a mathematical model due to the huge differences between the repeated experiments. Despite of this, two more experiments were conducted. In the first one, the cutting parameters providing a Ra of 1 nm, according to the literature, were used. These parameters are; a cutting speed of 90 m/min, a depth of cut of 1 µm and a feedrate of 1 mm/min [9, 11, 12, 15]. The results, attained using this set of cutting parameters, are given in Table 5.8. Secondly, the average values of the lower and the upper values of the cutting parameters were used. In this experiment cutting parameters were a cutting speed of 100 m/min, a depth of cut of 5 µm and a feedrate of 5 mm/min. The results of this experiment are given in Table 5.8.

Table 5.8 Measured Ra of a Surface Generated with Cutting Parameters V=90 m/min, d=1 µm, fr= 1 mm/min; Tool Rake Angle= -15°

Measurement Number	Mirror-like Region	Cloudy Region
1	1.5	21.9
2	2.5	17.2
3	2.7	18.3

According to the results seen in Table 5.8, 1 nm Ra could not be obtained with a tool rake angle of -15°. In addition, there is a big difference in average roughness values between the mirror like regions and the cloudy regions. The same situation is also valid for the results in Table 5.9.

Table 5.9 Measured Ra of a Surface Generated with Cutting Parameters V=100 m/min, d=5 µm, fr= 5 mm/min; Tool Rake Angle= -15°

Measurement Number	Mirror-like Region		Cloudy Region	
	Replicate 1	Replicate 2	Replicate 1	Replicate 2
1	2.7	1.4	11.4	18.9
2	2.3	1.6	5.8	17.6
3	1.5	1.7	8.2	17.6

5.3 Third Set of Experiments: Constant

The repeatability problem and formation of cloudy regions, in the second set forced to change the tool. In this set of experiments N020WG type tool, which has -25° rake angle was used. The tool parameters are given in Table 5.10. The cutting fluid, Clarisol 330 was used as the previous experiments.

Table 5.10 Cutting Fluid and Tool Parameters

Cutting Fluid	Clairsol 330
Tool	N020WG
Radius	0.50 mm
Rake	-25°
Clearance	10°

At the beginning, the first specimen was cut with a cutting speed of 240 m/min, a depth of cut of 1 µm and a feedrate of 10 mm/min. This set of parameters resulted with the patterns on the surface. Therefore, the feedrate was decreased until no cloudy regions were observed. It was found that 5 mm/min is the maximum feedrate. At this point, the depth of cut was increased until there cloudy regions appeared again. It was observed that 6 µm was the maximum depth of cut. Thus, 5 mm/min of feedrate and 6 µm of depth of cut were evaluated as upper values for

depth of cut and feedrate. The lower values for these parameters were selected as 1 µm and 1 mm/min, respectively. The cutting parameters used in this set of experiments and the measured Ra values are given in Table 5.11

Table 5.11 Cutting Conditions and Measured Ra Values in 3rd Set

Exp. Num.	V [m/min]	d [µm]	fr [mm/min]	Ra [nm] Msr.1	Ra [nm] Msr.2	Ra [nm] Msr.3	Ra [nm] Avg.
1	120	1	1	1.1	1.2	0.8	1.0
2	240	1	1	1.4	1.2	1.3	1.3
3	120	6	1	1.6	1.5	1.5	1.5
4	240	6	1	1.7	1.6	1.8	1.7
5	120	1	5	2.7	2.8	2.8	2.8
6	240	1	5	3.0	2.9	3.5	3.1
7	120	6	5	3.9	3.5	3.3	3.5
8	240	6	5	4.5	3.5	3.1	3.7

5.3.1 Estimation of Parameter Effect

The main and the interaction effects of cutting parameters are evaluated as given in Appendix F. The effect values are presented in Table 5.12. Considering the main effects, A- cutting speed is the least important one among the others, where C- feedrate has the most significant effect on the result. B-depth of cut can be interpreted as it has a more important effect on the result than cutting speed but, this influence is not as much as feedrate. The interaction effect of A-cutting speed and B-depth of cut factors is the least significant one. The Interaction effects including C-feedrate have considerable values. It is remarkable that, all the two factor interactions; AB, AC and BC, have negative values, which is unexpected. This can be interpreted as two factors interactions have decreasing effects on the

surface roughness. In contrast, three factors interaction has a positive effect on the result.

Table 5.12 Main and Interaction Effects on Ra

Effect	Value
A	0.3
B	0.5
C	1.9
AB	-0.1
AC	-0.7
BC	-0.7
ABC	0.9

5.3.2 Ra Prediction Formula

The prediction formula is derived using the inputs of the experiments; the cutting parameters and the outputs which are the Ra values of generated surfaces. The calculation details are given in Appendix F.

The formula derived is:

$$Ra = 0.14 + 2.667\times10^{-3}V + 0.11d + 0.44fr - 2.083\times10^{-4}Vd - 4.167\times10^{-4}Vfr + 5\times10^{-3}fd + 4.167\times10^{-5}Vdfr \quad (5.1)$$

where Ra (nm) is average roughness, V (m/min) is cutting speed, d (μm) is depth of cut and fr (mm/min) is feedrate. The change in Ra with respect to the cutting parameters is graphically represented in Figure 5.13-5.15.

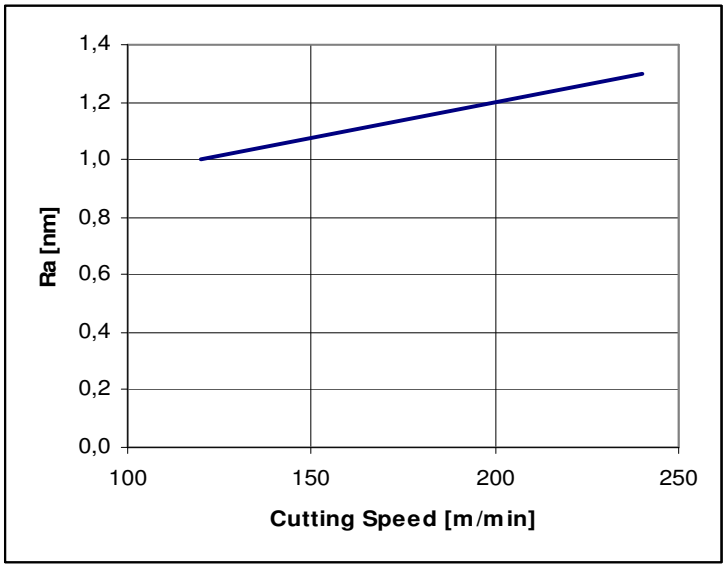

Figure 5.13 Ra vs. Cutting Speed

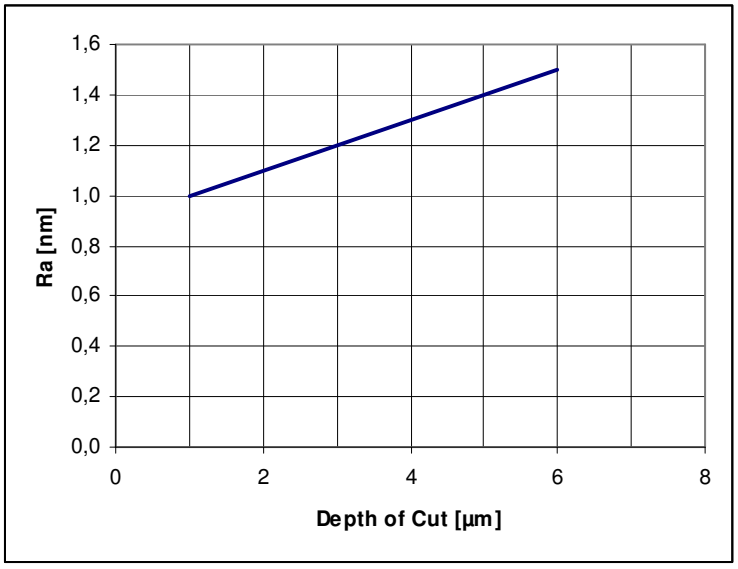

Figure 5.14 Ra vs. Depth of Cut

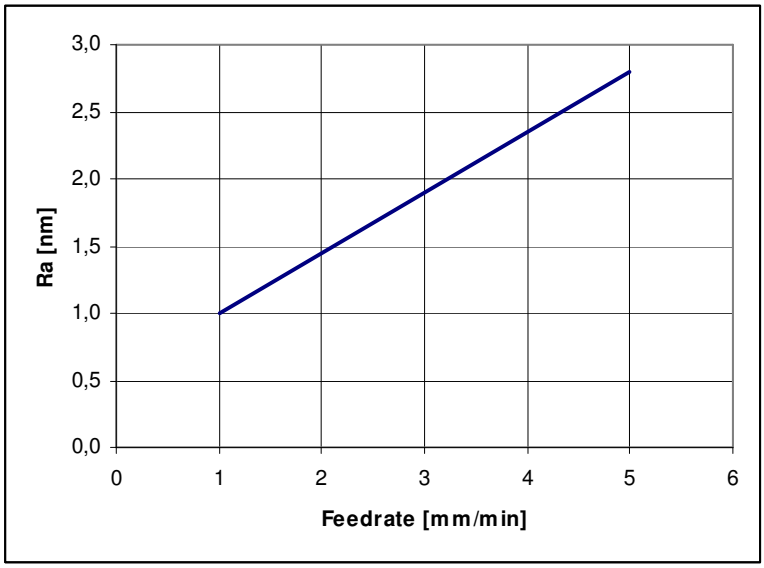

Figure 5.15 Ra vs. Feedrate

The prediction formula was tested with two control experiments. In the first control experiment a cutting speed of 180 m/min, a depth of cut of 3 µm and a feedrate of 2.5 mm/min were used. These values are the average of the upper and the lower values used in the experiments. In the second control experiment a cutting speed of 90 m/min, a depth of cut of 1 µm and a feedrate of 1 mm/min were used. The second set of cutting parameters are said to provide a Ra of 1 nm, in the literature[9, 11, 13, 15]. The cutting parameters and the results obtained using these sets of cutting parameters are given in Table 5.13.

The Ra values, for the cutting parameters of control experiments, were predicted by making use of Equation 5.1.The predicted Ra values and the errors in the predictions are given in Table 5.14.

Table 5.13 Cutting Conditions and Measured Ra Values Control Experiments

Experiment	V [m/min]	d [µm]	fr [mm/min]	Ra [nm] Msr.1	Ra [nm] Msr.2	Ra [nm] Msr.3	Ra [nm] Avg.
Control 1	180	3	2.5	1.7	2.2	1.8	1.9
Control 2	90	1	1	0.9	1.2	0.9	1.0

Table 5.14 Calculated Errors for Control Experiments

Experiment	Observed Ra [nm]	Predicted Ra [nm]	Error [nm]	Error %
Control 1	1.0	0.9	-0.1	-10
Control 2	1.9	2.0	0.1	-5

The results of the experiments are discussed in Section 5.4. However, it can be noticed that, using a depth of cut of 1 µm, a feedrate of 1 mm/min and a cutting speed of 90 m/min resulted a Ra of approximately 1 nm. This result is parallel with literature by Fang [12, 13] and better than the surface roughness obtained by Leung [15]. The measurements screens are given in Appendix G. Hence, it can be concluded that the prediction formula is valid for the selected range of cutting parameters. The maximum values of depth of cut and feedrate are proposed as the upper limits for finish cut of silicon. The formula cannot be used since the cutting regime differs beyond these values. The minimum values of depth of cut and feedrate are selected so small that, smaller values are not practically used for finish cut.

5.4 Discussion

5.4.1 Effect of Tool Rake Angle

Surface quality gets distinctly better when cutting with negative rake angle diamond tools. Negative rake angle produces a kind of compressing stress state in

front of the tool edge, which can prohibit the creation and propagation of cracks. In addition, negative rake angle is helpful to ductile cutting. Another study supporting the idea is by Yan [20]. In his work, it is suggested that performance of 0° rake angle diamond tool can be improved by adjusting the rake angle to a suitable negative value. On the contrary, there is a study which argumented that 0° tool rake angle has some advantages over -25° such as providing a more ductile [55].

Tool manufacturer's catalog recommends rake angles from -15° to -25 ° to machine silicon, as seen in Appendix C. However, in many studies the tool rake angle of was selected as-25° to investigate silicon machining [9, 19, 56].

In this study, comparing the second and the third sets of experiments, it can be deduced that, increasing the negative rake angle from -15° to -25° improved surface finish. This can be explained as in the study of Leung [15]. Increasing negative rake angle increases the maximum critical depth of cut in ductile regime. The result is also supported by the studies of Yu [11] and Zhou [19].

5.4.2 Effect of Spindle Speed and Cutting Speed

In the first set of experiments, the constant spindle speed was used. Cutting parameters and obtained results have been given in Section 5.1. It was observed that by using constant spindle speed, the required surface roughness values could be achieved. In this set of experiments, raising the spindle speed from 1000 rpm to 3000 rpm affected the surface roughness in a good manner. Besides, the experiments with 3000 rpm imply that cutting speed has no significant influence on surface roughness. Nevertheless, N=1000 rpm condition does not match this argument.

In the second and the third sets, the constant cutting speed was used. The effect estimation analysis using the data from the third set of experiments has shown that the cutting speed has the least important effect on the surface roughness. This result is also compatible with the results obtained in the first set of experiments. Furthermore, this argument is parallel to the literature [11, 57]

The constant cutting speed operation provides a homogenous cutting condition for the whole surface, regarding only the cutting speed parameter. The machine tool controls the spindle speed so that the cutting speed is kept constant. This can only be achieved by changing the spindle speed with respect to the cutting diameter. In Figure 5.16, the changing in the spindle speed with respect to the diameter, to provide a cutting speed of 120 m/min is given. The formulation of this change is given in Equation 2.1. Rearranging this equation,

$$N = \frac{V}{\pi D} \tag{5.2}$$

Thus, it is seen that the spindle speed is inversely proportional to the cutting diameter. Therefore, as the cutting diameter approaches to zero, the spindle speed tends to go to the infinity. Since infinite spindle speed is impossible, an upper limit, which is 3800 rpm, has to be set for spindle speed in the part program.

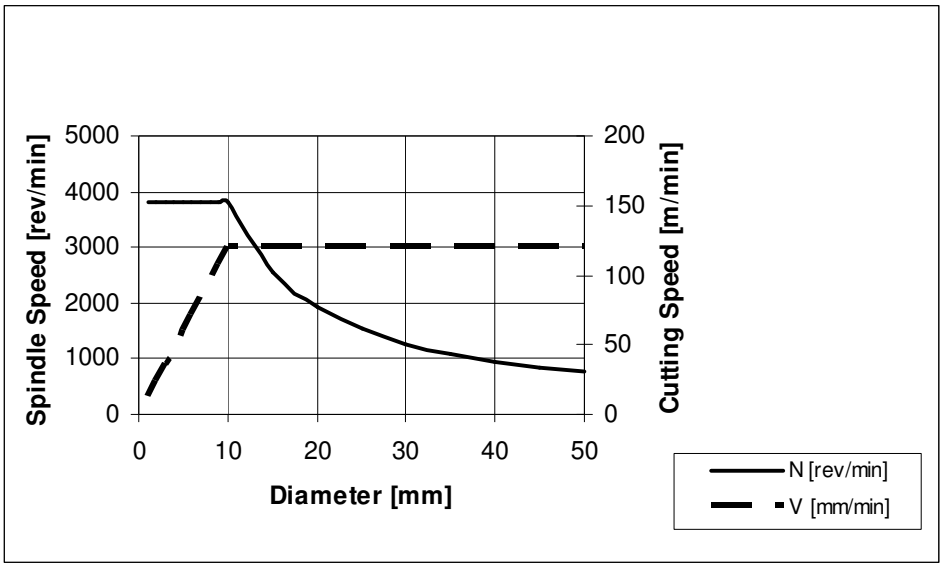

Figure 5.16 The Change in Spindle Speed in a Facing Operation with Constant Cutting Speed

5.4.3 Effect of Feedrate

The analysis carried out shows that feedrate is the most important factor in machining of silicon. In Table 5.14 it has been shown that increasing feedrate from 1 mm/min to 5 mm/min increased the average roughness by 1.7 nm, while other cutting parameters were kept at their minimum values.

The significance of feedrate, according to this study, shows conformity with the literature. Sreejith describes feedrate as the prime in ductile regime machining [18]. As it has been detailed in Chapter 2, feedrate determines the critical chip thickness which limits ductile regime machining.

Xiangdong [9] showed that increasing feedrate degrades the surface quality. In his work degradation is graphically represented as linear. However, it can be argued that exceeding the critical limit can increase the surface roughness enormously and unpredictably. An other conclusion about significance of feedrate is by Leung [15].

It is stated that, there exits a clear relationship between ductile regime machining and feedrate.

The crucial point about feedrate is its being dependent on spindle speed. The relation between feed and feedrate has been given in Equation 2.3. Rearranging this equation, it is obtained that

$$f = fr / N \tag{5.3}$$

According to the equation, the feed is directly proportional to the feedrate. On the other side, it is inversely proportional to the spindle speed. If constant feedrate is specified in a part program for a constant cutting speed in facing operation, the machine tool decreases the feed as the spindle speed increases towards the center of the specimen, in order to keep the feedrate constant. This relation is graphically represented in Figure 5.17. Because of this relation, the advancement of the tool (i.e. feed in radial direction) into the part differs with diameter. The outer regions are machined with bigger advancements of the tool, compared with the inner regions; even though the feedrate is kept constant. The difference in feed in radial direction causes roughness variations in the specimen. This problem is not encountered in the constant spindle speed facing operations. Hence, it can be deduced that regarding the minor influence of the cutting speed on roughness, the constant spindle speed can be used in facing operations to overcome this problem, since this provides constant feed in radial direction.

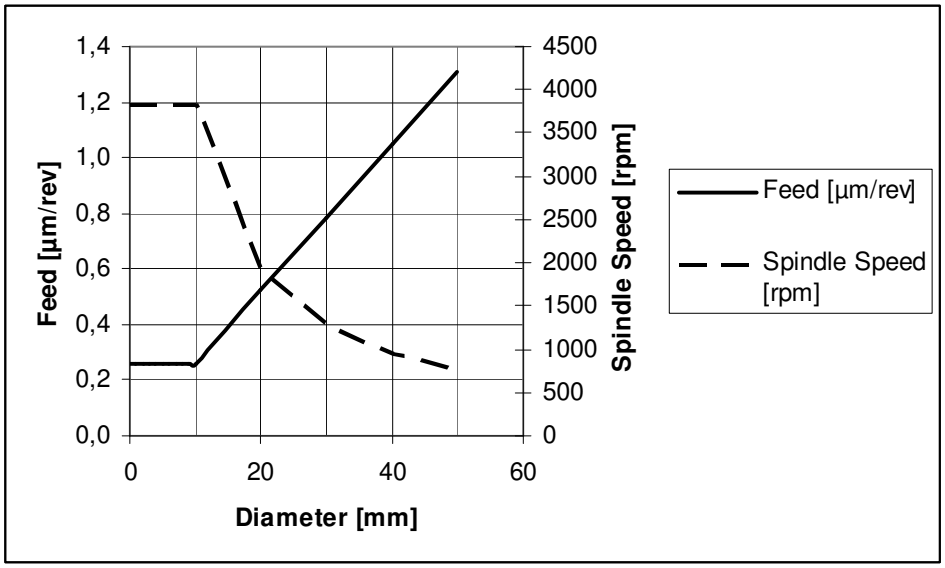

Figure 5.17 The Change in Feed in a Facing Operation with Constant Cutting Speed

5.4.4 Effect of Depth of Cut

In the analysis, it has been shown that effect of depth of cut is less effective than the effect of feedrate on the result. Increasing depth of cut from 1 µm to 6 µm increased the surface roughness by 0.6 nm, while other cutting parameters were kept at their minimum values.

The result obtained in this study is complies with the conclusion of Sreejith [18] mentioned in the section on the effect of feedrate. Leung [15] expressed that the surface finish had become very smooth as the depth of cut was below 5 µm. However, it was shown that a depth of cut of 10 µm had given damaged surface, even with a feedrate of 1 mm/min.

In the study of Yu [11], the depth of cut above 5 µm caused unacceptable surface quality Moreover, many studies show that, the best surface can be achieved by 1 µm depth of cut [9, 11, 13, 15].

CHAPTER 6

CONCLUSIONS AND FUTURE WORK

6.1 Conclusions

Silicon is widely used in manufacturing of infrared optics for thermal imagining systems which are especially utilized in military applications. In silicon optics production, single point diamond turning (SPDT) is considered to be a viable method for fabricating high quality surfaces.

In this experimental study, the effects of cutting parameters; cutting speed, depth of cut and feedrate, on single point diamond turning of optical grade silicon have been investigated. In experiments, mono crystalline silicon substrates with a diameter of 50 mm have been used. The study includes only finish cut experiments. Through out the study, beyond various cutting conditions, cutting tools with two different rake angles were utilized. Three sets of experiments have been realized by considering "2^3 factorial design method". A mathematical model between average roughness and cutting parameters has been established.

The general conclusions of this study on ultra-precision machining of optical grade silicon can be summarized as follows:

1. The first set of experiments was conducted with constant spindle speed. The lower and the upper values of the spindle speed were selected as 1000 rpm and 3000 rpm, respectively. The upper and the lower values for feedrate were 1 mm/min and 3 mm/min and for depth of cut 2 µm and 5 µm. It was observed that facing with 3000 rpm provided surface quality Ra values generally between 2nm and 5 nm. This range of average roughness is below the maximum acceptable Ra value of 25 nm.

2. In the second set of experiments constant cutting speed was used. The lower and the upper values for cutting speed were selected as 50 m/min and 150 m/min. The lower value of feedrate was 1 mm/min and its upper value was 10 mm/min. The depths of cut values were 1 µm and 10 µm. The rake angle of the tool was –15°. In this set of experiments, unrepeatable Ra values were obtained. Most of the measured Ra values were above the acceptable Ra limit, which is 25 nm. In addition, cloudy region patterns were observed. The patterns observed are similar to the ones described in Chapter 2 and literature [35, 36]. It is concluded that material orientation is important for optics manufacturing and it must be specified in technical documents used for purchasing of silicon material.

3. The third set of experiments was conducted with constant cutting speed. The values for cutting speed were 120 m/min and 240 m/min. The feedrate values were 1 mm/min and 5 mm/min. The values selected for depth of cut were 1 µm and 6 µm. The results of this set could be used for building a mathematical model for prediction. The empirically derived prediction formula is,

$$Ra = 0.14 + 2.667\times10^{-3}V + 0.11d + 0.44fr - 2.083\times10^{-4}Vd$$
$$- 4.167\times10^{-4}Vfr + 5\times10^{-3}fd + 4.167\times10^{-5}Vdfr$$

where

Ra : Average Roughness [nm]

V : Cutting Speed [m/min]

d : Depth of Cut

fr : Feedrate

In order to test this formulation, two additional experiments were carried out. As a result these experiments, it was seen that the formulation is valid within the specified ranges. On the other hand, in parallel with literature it was seen that, using a cutting speed of 90 m/min, a depth of cut of 1 µm and a feedrate of 1 mm/min provides average surface roughness of about 1 nm.

The following tool features and cutting parameters by using constant cutting speed mode are recommended as a result of this particular study;

Tool Radius: 0.50 mm
Tool Rake Angle: -25°
Cutting Speed: 120-240 m/min
Depth of Cut: 6 µm
Feedrate: 5 mm/min

4. It was observed that, a cutting tool with a rake angle of -25° is more appropriate than a cutting tool with a rake angle of -15°, for cutting optical grade silicon.

5. Feedrate is figured out to be the most effective parameter on surface roughness. Increasing feedrate degrades surface quality. Thus, it is beneficial to use the maximum feedrate which provides acceptable surface quality for time saving. In this study, surface qualities with Ra better than 5 nm have been obtained by employing a feedrate of 5 mm/min. This surface quality is within accepted surface quality, which is Ra= 25 nm. When the recommended feedrate of 2.5 mm/min is considered, the machining time is reduced by 50%, by using a feedrate of 5 mm/min.

6. It is concluded that cutting speed is the least effective cutting parameter on surface quality of silicon. Besides, most ultraprecision machine tools, like the one used in this study, cannot perform operations with constant cutting speed and constant feed [mm/rev] at the same time. Therefore, machining with constant spindle speed is recommended. Using constant spindle speed in facing operation provides uniform advancement of the tool per revolution through the diameter of the specimen.

7. It is difficult to predict ultra-precision machined surfaces. In dealing with nano level roughness values, deviations of few nanometers affect the result in a great manner.

6.2 Future Work

Some proposed future works to this study can be given as follows:

1. In this study, only the cutting tools with -15° and -25° rake angles were used. Effects of employing different rake angles regarding surface finish, tool wear, machining economy may be analyzed. A prediction formula can be pursued using different rake angle tools.

2. Effect of lubricant, which was not included in this study, is another important parameter for micromachining,. Therefore the effects of different lubricants can be investigated.

3. Tool wear is an important factor for surface finish. Besides, it is significant from economic aspects. Not only cutting parameters but also tool angles influence tool wear. Hence, tool wear in silicon machining may be studied in order to determine the most economically efficient cutting conditions.

4. It is known that some critical frequencies may induce chatter during machining. The critical frequencies and stiffness of machine tool can be analyzed. Besides, the fluctuations in power supply and vacuum supply of the system may also be effective on the machining. The effects of these parameters on the system can be studied.

5. Chip formation in silicon can also be studied in order to develop a better understanding of the ductile regime cutting.

6. Time and cost optimization of silicon optics manufacturing can be studied in order to determine the optimum cutting conditions for minimum time or minimum cost considerations.

7. A similar study can be carried out for spherical and aspherical surfaces.

REFERENCES

1. Aselsan. 5 May 2007. <www.aselsan.com.tr>
2. BMW. 18 August 2007. <http://www.bmw.com.au>
3. *IR Energy, ASELSAN MGEO Group, Education Notes*.
4. Colorado University. 3 August 2007. <http://lasp.colorado.edu/>
5. *Infrared Technology, ASELSAN MGEO Group, Education Notes*.
6. Infrared, Inc. 23 June 2007. <http://www.infrared.com>
7. Matweb. 12 April 2007. <http://www.matweb.com>
8. Silicon. <http://www.almazoptics.com/Si.htm>
9. Xiangdong, L., *Ultra-precision Turning Technology*, P.T.D. Precision Machining Group, Editor. 2000, Singapore Institute of Manufacturing Technology.
10. N.Ikawa, et al., *Ultraprecision Metal Cutting - Past, the Present and the Future.* Annals of CIRP, 1991. 40(2): p. 587-594.
11. Yu, J. and J. Yan, *Ultraprecision Diamond Turning of Optical Crystals.* SPIE, 1994: p. 51-59.
12. F.Z.Fang, *Nano-turning of single crystal silicon.* Journal of Materials Processing Technology, 1998. 82: p. 85-101.
13. F.Z.Fang and V.C.Venkates, *Diamond Cutting of Silicon with Nanometric Finish.* Annals of the CIRP, 1998. 47(1): p. 45-50.
14. Morris, J.C., et al., *Origins of the Ductile Regime in Single-Point Diamond Turning of Semiconductors.* Journal of American Ceramic Society, 1995. 78(8): p. 2015-2020.
15. Leung, T.P., W.B.Lee, and X.M.Lu, *Diamond Turning Of Silicon Substrates in Ductile Regime.* Journal of Materials Processing Technology, 1998. 73: p. 42-48.

16. Blake, P.N. and R.O. Scattergood, *Crystal Orientation Dependence of Machining Damage- a Stress Model.* Journal of American Ceramic Society, 1990. 73(949): p. 3113-3115.

17. Sreejith, P.S. and B.K.A.Ngoi, *Machining Force Studies on Ductile Machining of Silicon.* Journal of Materials Processing Technology, 2005. 169: p. 414-417.

18. Sreejith, P.S. and B.K.A. Ngoi, *New Materials and Their Machining.* The International Journal of Advanced Manufacturing Technology, 2001. 18: p. 537-544.

19. Zhou, M., et al., *Brittle- Ductile Transition in Diamond Cutting of Silicon Single Crystals.* Materials and Manufacturing Processes, 2001. 16(4): p. 447-460.

20. Yan, J., et al., *Ductile Regime Turning at Large Tool Feed.* Journal of Materials Processing Technology, 2002. 121: p. 363-372.

21. Chao, C.L., et al., *Ductile Behavior in Single Point Diamond Turning of Single Crystal Silicon.* Journal of Materials Processing Technology, 2002. 127: p. 187-190.

22. Hung, N.P. and Y.O. Fo, *Effect of Crystalline Orientation in Ductile Regime Machining.* The International Journal of Advanced Manufacturing Technology, 2000. 16: p. 871-876.

23. Stephenson, D.A. and J.S. Agapiou, *Metal Cutting Theory and Practice*. 2006, Boca Raton: CRC Press.

24. Boothroyd, G. and W.A. Knight, *Fundamentals of Machining and Machine Tools*. 1989, New York: Marcel Dekker Inc.

25. Taniguchi, N., *Current Status in, and Future Trends of Ultra-precision Machining and Ultra-fine Materials Processing.* Annals of CIRP, 1983. 32(2): p. 573-582.

26. Trent, E.M., *Metal Cutting*. 1991, Oxford: Butterworth-Heinemann Ltd.

27. Contour Fine Tooling. 2 August 2007. <www.contour-diamonds.com>

28. Michigan Technical University, Mechanical Engineering Department 16 July 2007. <http://www.me.mtu.edu/>

29. Smith, W.F., *Principles of Materials Science and Engineering*. 1990, New York: McGraw-Hill, Inc.

30. Dieter, G., *Mechanical Metallurgy*. 1986, New York: McGraw-Hill.

31. Caltech University. 15 June 2007. <http://design.caltech.edu/>

32. Laboratory for Scientific Visual Analysis. 17 March 2007. <http://www.sv.vt.edu>

33. Lecture Notes on Metal Cutting. 30 August 2006. <http://www.me.metu.edu.tr/me535/>

34. Blake, P.N. and R.O. Scattergood, *Ductile-Regime Machining of Germanium and Silicon.* Journal of the American Ceramic Society, 1990. 73(4): p. 949-957.

35. O'Conner, B.P., E.R. Marsh, and J.A. Couey, *On the Effect of Crystallographic Orientation on Ductile Material Removal in Silicon.* Precision Engineering, 2005. 29: p. 124-132.

36. Blackley, W. and R.O. Scattergood, *Crystal Orientation Dependence of Machining Damage- A Stress Model.* Journal of American Ceramic Society, 1990. 73(949): p. 3113-3115.

37. Çelik, A., *Development of a Metrology for Prediction of Surface Roughness of Curved Cavities Manufactured by 5-Axis CNC Milling*, in *Mechanical Engineering*. 2007, Middle East Technical University: Ankara.

38. Precision Devices, Inc. . 9 May 2007. <http://www.predev.com/>

39. Turkish Standards Institution. 12 December 2007. <http://www.tse.org.tr>

40. Karabay, M., *Lecture Notes on Engineering Metrology and Quality Control*. 2003, Ankara: Middle East Technical University, Mechanical Engineering Department.

41. Thomas, T.R., *Rough Surfaces*. 1982, New York: Longman.

42. Mahr Federal Inc.,. 10 September 2007. <http://www.mahr.com>

43. The. Sutherland Research Page. 12 September 2007. <www.mfg.mtu.edu>

44. Taylor Habson, Inc. 26 October 2007 <http://www.taylor-hobson.com>

45. Thomas, T.R., *Rough Surfaces*. 1999, London: Imperial College Press.

46. College of Optical Sciences. 26 May 2006. http://www.optics.arizona.edu>

47. Ltd., T.H., *Exploring Rough Surfaces*. 2003: Taylor Hubson Ltd.

48. Precitech Inc. 10 June 2007. <http://www.precitech.com/>

49. *Nanoform 350 Operator's Manual*: Precitech Inc.

50. Zygo Corporation. 17 July 2007. <www.zygo.com>

51. İlkgün, Ö., *Effects of Production Parameters on Porosity and Hole Properties in Laser Sintering Rapid Prototyping Process*. 2005, Middle East Technical University: Ankara, Turkey.

52. Krulewich, D.A., *Experimental Design for Single Point Diamond Turning of Silicon*. 1996, Lawrence Livermore National Laboratory.

53. Montgomery, D.C., *The 2k Factorial Design, Design and Analysis of Experiments*. 2004, New York: John Wiley & Sons.

54. Personal communication in Aselsan Inc.

55. Patten, J.A. and W. Gao, *Extreme Negative Rake Angle Technique For Single Point Diamond Nano-Cutting of Silicon.* Precision Engineering, 2001. 25: p. 165-167.

56. Cheung, C.F., *Influence of Cutting Friction on Anisotropy of Surface Properties in Ultra-Precision Machining of Brittle Single Crystals.* Scripta Materialia, 2003. 48: p. 1213-1218.

57. Sreejith, P., et al., *Recent Advances in Machining Silicon Wafers for Semiconductor Applications.* International Journal of Advanced Manufacturing Technology, 2001. 17(2): p. 157-162.

58. Siliconfareast. August 2007. <http://www.siliconfareast.com>

59. Montgomery, D.C., *Design and Analysis of Experiments*. 2001, New York: John Wiley & Sons.

APPENDIX A

NANOFORM 350 ULTRAPRECISION MACHINING SYSTEM

Nanoform 350 is a machining system manufactured by Precitech, Inc. Nanoform 350 is a 2 axis diamond machining system designed for precision manufacturing of optics, optical molds and mechanical components in ferrous and nonferrous materials.

The systems is on sealed natural granite base to eliminate machine contamination. Self leveling isolation system minimizes vibration influences during machining. The system is driven by linear motors and hydrostatic oil bearing slideways with advanced stiffness characteristics provide ultimate performance.

Nanoform 350 is equipped with a spindle, which provides 25 nm motion accuracy. The feedback resolution of the machining system is 1.4 nm. Additionally, the programming resolution is 1.0 nm.

Properties of the machining system can be summarized as follows:
Slide Trave: X-350 mm , Z-250 mm
Maximum Feedrate: 1500 mm/min
Swing Capacity: 350 mm
Load Capacity: 68 kg
Workholding Spindle Speed: ≤5000

Table A.1 Nanoform 350 Machine Technical Specifications

precitech	Rev. 0206	Nanoform® 350/700 Machine Technical Specification		
Machining Systems	Nanoform® 350 and Nanoform 700 Specification criteria			
Base/Control	**Machine Type**	**Multi-Axis Contouring System**		
	Machine Base	Natural, high-stability, fullysealed, impala granite/steel frame		
	Vibration Isolation	Self leveling dual chamber vibration isolation		
	Control System	UPx 1.0 - 1.0nm Resolution		
	Operating system	QNX Rev. 4.0		
	Swing Capacity	**N350-** 350mm (14") diameter - with riser: 450mm (18")	**N700-** 700mm (28") diameter - with riser: 1016mm (41")	
	SPDT Performance	Typical results from standard test sample - **Surface Roughness** - 2.0nm RA **Form Accuracy** - 0.1µm P-V		
Slideway Design	**Type**	**Hydrostatic Box-type Slideways**		
	Material	DuraBar Cast Iron		
	X -Travel	350mm (14")		
	Z -Travel	250mm (10")		
	Maximum feedrate	1500mm/min. (59"/min.)		
	Drive system	AC Linear Motor		
	Position Feedback Resolution	8.6 or 1.4nm		
	X-Axis straightness Horz.	0.3µm (12µ")		
	Z-Axis straightness Horz.	0.3µm (12µ")		
	X- Vertical / Horizontal Stiffness	438 N/µm / 438 N/µm (2,500,000 lbs/in.)		
	Z- Vertica l/ Horizontal Stiffness	438 N/µm / 438 N/µm (2,500,000 lbs/in.)		
Workholding Spindles	**C-Axis/ Workholding Spindles**	Standard: **Precitech SP150 Spindle**	Optional: **Precitech NT151 Spindle**	Optional: **Precitech SP75 Spindle**	Optional: **Professional Instruments 5.5**
	Type	**Precitech built** Air bearing spindle with slot type thrust bearing.			Groove compensated air bearing
	Material	Steel shaft/bronze journal			Steel shaft/aluminum anodized journal
	Load capacity @ nose / 50mm (2") out	68Kg (150 lbs) / 48Kg (105 lbs)	68Kg (150 lbs) / 57Kg (125 lbs)	18 Kg (40 lbs.) /	46Kg (101lbs.) /
	Axial stiffness @ 100 PSIG	228 N/µm (1,300,000 lbs/in.)	261 N/µm (1,500,000 lbs/in.)	70 N/µm (400,000 lbs/in.)	140N/µm (800,000 lbs/in.) @120 PSI
	Radial stiffness @ 100 PSIG @ spindle nose	88 N/µm (500,000 lbs/in.)	105 N/µm (600,000 lbs/in.)	22 N/µm (125,000 lbs/in.)	88 N/µm (500,000 lbs/in.)@ 120PSI
	Motion accuracy	Axial/Radial ≤ 25nm (1µ")	Axial/Radial ≤ 50nm (2µ")	Axial/Radial ≤ 50nm (2µ")	Axial/Radial ≤ 25nm (1µ")
	Thermal control	Liquid cooled motor housing /Journal bearing			
	Drive amplifier	DC Brushless Sin Drive			3-phase DC Brushless
	C-axis feedback resolution	0.05 - 0.72 arc-sec	0.13 - 2.16 arc-sec	0.05 - 0.72 arc-sec	0.06 arc-seconds
	C-axis position accuracy	+/- 2.0 arc-sec			
	C-axis maximum speed	275 RPM	800 RPM	275 RPM	2000 RPM
	Workholding spindle maximum speed	2500/5000/7000 RPM	6000 RPM	15,000 RPM	10,000 RPM
	Included features	Mechanical locking mechanism, non-influencing vacuum feed through			
Tooling Spindles	**High Speed Tooling Spindles**	Standard: **Precitech SP75FF Spindle**		Optional: **Professional Instruments 2.25**	
	Type	**Precitech built** Air bearing spindle with slot type thrust bearing.			
	Material	Steel shaft/Bronze journal		Steel shaft/Aluminum anodized journal components	
	Maximum speed	15,000 RPM		50,000 RPM	
	Standard swing capacity	125mm Diameter.			
	Load capacity @ nose / 50mm (2") out	18 Kg (40 lbs.) / 11Kg (25 lbs.)		20Kg (44 lbs.) /	
	Axial stiffness @ 100 PSIG	70 N/µm (400,000 lbs/in.)		68.6 N/µm (392,000 lbs/in.)	
	Radial stiffness @ 100 PSIG @ spindle nose	26 N/µm (150,000 lbs/in.)		22.6 N/µm (130,000 lbs/in.)	
	Motion accuracy	Axial/Radial ≤ 50nm (2µ")		Axial/Radial ≤ 50nm (2µ")	
	Mounting location	Vertical, horizontal, 45 degree or on Rotary B-axis		Vertical, horizontal, 45 degree or on Rotary B-axis	
	Thermal control	Liquid cooled motor housing/Journal Bearing		Liquid cooled motor housing	
	Drive amplifier	3-phase		3-phase	
Rotational B-Axis	**Rotary B-Axis**	**Precitech HydroRound B-Axis SMALL** (N350)		**Precitech HydroRound B-Axis LARGE** (N700)	
	Type	Bi-conical, self compensated, oil hydrostatic		Bi-conical, self compensated, oil hydrostatic	
	Material	High-Alloy Steel		High-Alloy Steel	
	Standard swing capacity	200mm (8") Diameter.		300mm (12") Diameter.	
	Load capacity (limited by Z table)	225Kg (500 lbs.) (safety factor of 3)		455Kg (1000 lbs.) (safety factor of 6)	
	Axial stiffness	525 N/µm (3,000,000 lbs/in.)		1750 N/µm (10,000,000 lbs/in.)	
	Radial stiffness	175 N/µm (1,000,000 lbs/in.)		525 N/µm (3,000,000 lbs/in.)	
	Motion accuracy	Axial/Radial ≤ 0.10µm (4µ").		Axial/Radial ≤ 0.10µm (4µ").	
	Coning Error	1.0nm/mm (1.0µ"/in.)		1.0nm/mm (1.0µ"/in.)	
	Drive amplifier	3-phase		3-phase	
	Feedback resolution	Available 0.036-0.36 arc-sec		Available 0.027-0.27 arc-sec	
	Position accuracy	+/- 2.0 arc-sec (compensated)		+/- 2.0 arc-sec (compensated)	
	Maximum speed	10 RPM continuous - 50 RPM Intermittant		10 RPM continuous - 50 RPM Intermittent	
Utilities	**Machine Utilities**	**Nanoform® 350 and Nanoform® 700 Platform**			
	Power	208 or 230VAC -1 phase - 50/60Hz			
	Air supply	Typical: 12 SCFM @100PSIG			
	Floor space - machine footprint	1930mm x 1220mm x 2043mm (76" x 48" x 80")			
	Floor space - w/control/peripherals	2930mm x 3807mm x 2043mm (115" x 150" x 80")			

APPENDIX B

AN EXAMPLE PART CODE USED IN THE STUDY

Silicon Machining

```
;  Job description: : silicon-No20 WG
;  Calculated maximum tool radius: 10000000000.000000
;  Total SAG (z_start - z_end) of all segments: 0.000000
;  Tool radius: 0.50000
;  Tool top rake angle (deg.): -25.000000
;  Tool clearance angle (deg.): 10.000000
;  Tool offset angle (deg.): 0.000000
;
g90
g18
g01
M3
g96S100        ;rough cut speed (V)
G92S3500       ;maks. spindle speed
x27z3F500
m7.2
x27z0F10       ;rough cut feed (f)
X0Z0
g04f0.5
z1F10
x27F100
G96S240        ;1. section cutting speed hizi (V)
Z-0.001F6      ;1. section depth of cut (d)
X15F5          ;1. section feed (f)
Z1F10
X15.6
G96S120        ;2. section cutting speed hizi (V)
G04F6
z-0.001
X0f6           ;2. Bolge feed (f)
G04F0.5
Z1F10
Z3F500
m9
X27
```

APPENDIX C

DIAMOND TOOLS

Tool numbering system of Contour Fine Tooling Company and suggested tool rake angles for different materials are given in Table C.1 and C.2, respectively.

Table C.1 Tool Numbering System

(S/M)	* (1 Character)	S= Sumitomo M= Monodyne No prefix if natural diamond is used
C	* (1 Character)	Type of Tool Radius C: Controlled N: Non-controlled
020(M)	*** (3 Character)	Radius Size e.g. 020= .020" e.g. 050M= 0.50 mm
L	* (1 Character)	See Table C.2
F	* (1 Character)	Front Clearance E= 15° F= 12.5° G= 10° H= 7.5° J= 5°
(C)	* (1 Character)	If "C" is stated conical clearance
(i)	* (1 Character)	If "i" is stated insert system

Table C.2 Suggested Tool Rake Angles for Different Materials

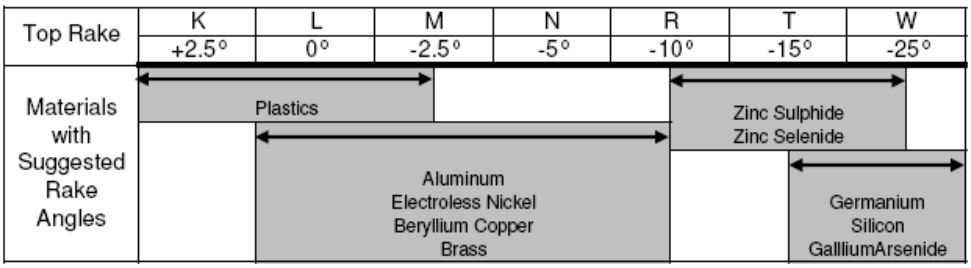

APPENDIX D

CUTTING FLUIDS

Clairsol 330 is a trademark of Petrochem Carless,Inc. In Table D.1 propertied of Clairsol 330 and some other cutting fluids are given

Table D.1 Properties of Different Cutting Fluids

	ALIPHATICS									
	WHITE SPIRIT AND SPECIAL KEROSINES									
	Clairsol 310	330	350	360	Odourless Kerosine	White Spirit	White Spirit 115	PD 260	Presol 110	130
Density @15°C	0.775	0.806	0.804	0.823	0.795	0.775	0.777	0.787	0.797	0.806
Flash point Abel °C	42	65*	76*	104*	80*	39	48	43	47.5	59
Aniline pt °C	73.1	69.7	74.9	78.9	75.0	56.8	58.1	59.2	61.0	63.6
Initial boiling point °C	163	195	200	241	205	153	166	156	160	170
Dry boiling point °C	194	220	260	270**	240	198	192	245	281**	292**
Aromatics % vol	0.3	0.13	0.8	NIL	0.8	16.3	17.8	14.2	17	18.6
Benzene content ppm	0	0	0	0	0	9	5	1	1	1
n-Hexane content ppm	0	0	0	0	0	<10	<10	<10	<10	<10
Bromine index mg/100g	<100	<100	<100	<100	<100	<500	<500	<500	<500	<500
Colour Saybolt	+30	+30	+30	+30	+30	+30	+30	+30	+25	+18
Refractive index @20°C	1.430	1.437	1.442	1.441	1.441	1.432	1.435	1.449	1.448	1.449
Litres/tonne	1290	1241	1244	1215	1258	1290	1287	1241	1225	1241

APPENDIX E

NEW VIEW 5000 INTERFEROMETER SPECIFICATIONS

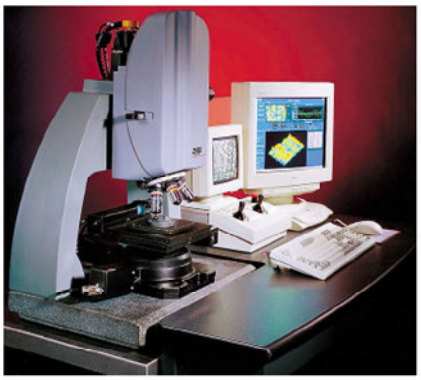

MODELS	
5010	Base model with high resolution camera and open loop transducer
5022	Model 5010 plus turret compatible and closed loop transducer
5032	Model 5022 plus high speed camera

SYSTEM	
Measurement Technique	Non-contact, three-dimensional, scanning white light and optical phase-shifting interferometry
Objectives	Infinite conjugate interferometric objectives; 1X, 2X, 2.5X, 5X, 10X, 20X, 50X, 100X
Image Zoom	Standard; continuous variable zoom with six indexed positions: 0.4, 0.5, 0.8, 1.0, 1.3, 2.0; repeatable to 0.2%
Field of View	From 0.04 to 17.5 millimeters; larger area imaged with field stitching; objective dependent; see Objective Specifications
Part Viewing	Standard; 9-inch b&w monitor
Focus	Standard; motorized manual and auto focus
Illuminator	Filtered white light with selectable coherence, long-life tungsten halogen lamp
Measurement Array	Standard, selectable, include: 640x480, 320x240, 160x120
Sample Stages	Manual and motorized versions available; see Options
Computer	Late-generation Dell PC configured with hard drive, 500 MB RAM, CD-R/W, floppy drive, and 17-inch flat panel monitor; printers optional
Software	Zygo MetroPro software running under Microsoft Windows 2000

PHYSICAL	
Dimensions (H x W x D)	System: 62 x 52 x 35 in. (157 x 132 x 89 cm) NewView 5000: 32 x 23 x 16 in. (81 x 58 x 41 cm) Vibration Isolation Table: 30 x 24 x 24 in. (76 x 61 x 61 cm) Workstation: 33.5 x 52 x 35 in. (85 x 132 x 89 cm)
Weight	System: ≈ 950 lb (430 kg) NewView 5000: ≈ 200 lb (90 kg) Vibration Isolation Table: ≈ 600 lb (272 kg)

PERFORMANCE	
Scanner	Model 5010: Open-loop piezo-based transducer Models 5022 and 5032: Closed-loop piezo-based, with highly linear capacitive sensors
Vertical Scan Range	Model 5010: 100 µm (3937 µin) Models 5022 and 5032: 150 µm (5906 µin) Optional up to 5 mm (0.20 in.)
Vertical Resolution	Up to 0.1 nm (0.004 µin)
Lateral Resolution	0.45 to 11.8 µm; objective dependent
Data Scan Rate	Models 5010 and 5022: up to 4.9 µm/sec Model 5032: up to 10.5 µm/sec; rate depends upon sampling array
Maximum Data Points	307,200; dependent upon sampling array
Step Height Accuracy	Model 5010: ≤ 3.0% Models 5022 and 5032: ≤ 0.75%
Step Height Repeatability	Model 5010: ≤ 1.5% @ 1σ Model 5022: ≤ 0.5% @ 1σ Model 5032: ≤ 0.1% @ 1σ

UTILITY REQUIREMENTS	
Input Voltage	100 to 240 VAC, 50/60 Hz
Power Consumption	≤ 280 watts (manual stages), ≤ 400 watts (motorized stages)
Compressed Air	60 to 80 psi (4.1 to 5.5 bar); 1/4 in. input; dry and filtered source (1% humidity, 5 µm particulate filter)

ENVIRONMENTAL REQUIREMENTS	
Temperature	15 to 30°C (59 to 86°F)
Rate of Temp. Change	<1.0°C per 15 min
Humidity	5 to 95% relative, noncondensing
Vibration Isolation	Required for vibration frequencies in the range of 1 Hz to 120 Hz

NewView™ 5000 Specifications

Options	
Stages	Manual Tip/Tilt/X/Y with ±6° tip/tilt, ±2 in. x/y, 230° rotation Motorized Tip/Tilt/X/Y with ±4° tip/tilt, ±3 in. x/y Motorized Tip/Tilt/Y/Theta with ±4° tip/tilt , y/theta with 3 in. y travel and 360° rotation
Objectives	Standard: 1X, 2.5X, 5X, 10X, 20X, 50X, 100X; LWD versions: 2X, 5X, 10X
Turrets	Model 5010: Single objective dovetail mounting Models 5022 and 5032: Manual or Motorized 5-position turret
Vibration Isolation	Vibration Isolation System recommended
Filters Sets	Standard, Rough surface, and Combination filter sets
Standards	NIST traceable step height standards; lateral calibration standards; precision reference flat

Test Part Characteristics	
Material	Various; opaque and transparent surface; coated and uncoated; specular and nonspecular
Preparation	None (typically); measurements are noncontact and nondestructive and performed under ambient conditions
Maximum Size (H x W x D)	3.5 x 8 x 8 in. (89 x 203 x 203 mm); larger sample sizes accommodated with special configurations
Reflectivity	1 – 100%
Roughness	Model 5010: ≤ 100 µm Rp standard Model 5022 and 5032: ≤ 150 µm Rp standard; Slope dependent; see Objectives

Nominal Objective Specifications at 1X*

Power	1X	2X LWD	2.5X	5X	5X LWD	10X	10X LWD	20X	50X	100X
Sys Mag	20X	40X	50X	100X	100X	200X	200X	400X	1000X	2000X
NA	0.030	0.055	0.075	0.130	0.140	0.300	0.280	0.400	0.550	0.800
Working Dist (mm)	8.5	20.5	10.3	9.3	20.5	7.4	18.8	4.7	3.4	0.55
Focus Depth (µm)	±322.5	±95.0	±51.6	±17.2	±14.8	±3.2	±3.7	±1.8	±1.0	±0.5
Inter Depth (µm)	4.0	4.0	4.0	4.0	4.0	4.0	4.0	3.6	2.0	1.0
Lateral Res (µm)	11.8	6.43	4.72	2.72	2.53	1.18	1.26	0.88	0.64	0.45
Field of View H x V (mm)	7.00 x 5.30	3.52 x 2.64	2.82 x 2.11	1.41 x 1.06	1.41 x 1.06	0.70 x 0.53	0.70 x 0.53	0.35 x 0.26	0.14 x 0.11	0.070 x 0.053
Spatial Samp 320 x 240 (µm)	22.00	11.0	8.80	4.40	4.40	2.20	2.20	1.10	0.44	0.22
Spatial Samp 640 x 480 (µm)	11.00	5.50	4.40	2.20	2.20	1.10	1.10	0.55	0.22	0.11
Max Slope (degree)	1.41	2.58	3.52	6.08	6.55	13.82	12.93	18.15	24.27	33.25

Nominal Objective Specifications at Other Zoom Settings

The NA, Working Distance, Focus Depth, Inter Depth, and Lateral Res specifications are the same at all zoom settings. Use the multipliers in the table below for Sys Mag, Field of View, and Spatial Samp specifications; multiply the value in the above chart times the multiplier.

Zoom Setting	*0.4*	*0.5*	*0.8*	*1.0*	*1.3*	*2.0*
Multiplier for Sys Mag	0.4	0.5	0.8	1.0	1.3	2.0
Multiplier for Field of View and Spatial Samp	2.5	2.0	1.25	1.0	0.77	0.5

***Objective Terminology**

Power	Magnifying power of the objective. LWD indicates Long Working Distance.
Sys Mag	System magnification, the enlargement of the surface as viewed on the video monitor.
NA	Numerical aperture, a number representing the resolving power of the objective.
Working Distance	The distance from the end of the objective to the test surface when focused.
Focus Depth	Vertical distance within which any specimen detail will simultaneously be in focus. The coherence bandwidth is centered within the focus depth.
Inter Depth	Interference depth, vertical distance over which interference can occur.
Lateral Res	Lateral resolution, optical resolution of the imaging system.
Field of View	The size of area imaged and measured.
Spatial Samp	Spatial sampling, the apparent pixel size at each magnification; varies based on Camera Res.
Max Slope	Maximum practical angle of surface feature from one pixel to the next that can be measured; will vary based on part and measurement attributes.

APPENDIX F

2^k FACTORIAL DESIGN

Factorial design is widely used in research work. Since number of factors, namely the parameters can vary; the general for m of the factorial design is 2^k factorial design. These experiments involve k factors, each at only two levels. “These levels may be quantitative, such as two values of temperature, pressure, or time; or they may be qualitative, such as two machines, two operators, the “high” and the “low” levels of factors, or perhaps the presence and absence of a factor. A complete replicate of such a design requires 2x2x2x…x2=2^k factorial design.

In order to put the methodology of factorial design, the case where k=2 is appropriate. Two factors, say A and B, each at run at two levels. This is called “2^2 factorial design”. The effect of each factor on the output can be due to itself, the main effect of the factor, or a result of the interaction between the factors [58]. In other words; the effect of a factor is defined as the change in response produced by a change in the level of the factor. This is called main effect because it refers to the primary factors of interest in the experiment [51]. And the interaction effect is the average difference between the effect of A at the high level of B and the effect of A at the low level of B [59].

In Figure F.1 the lowercase letter denotes that, during the application that factor is in its higher level and the “1” means that factor is in its lower level. For example “b” denotes that the factor B is at higher level and Factor A is at lower level. Also “1” is used to denote that all the factors are in their lower level. Where “n” is the number of replicates.

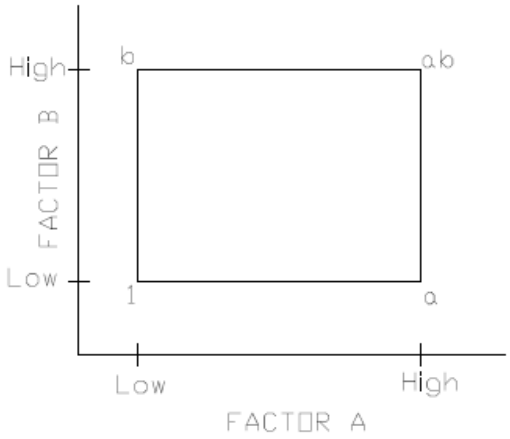

Figure F.1 Treatment Combinations in 2^2 Design

The main effect of factor A in this two level design is;

$$A = \frac{a + ab}{2n} - \frac{(1) + b}{2n} \tag{F.1}$$

The main effect of factor B in this two level design can be similarly calculated.

$$B = \frac{b + ab}{2n} - \frac{(1) + a}{2n} \tag{F.2}$$

The effect of the interaction between factors A and B (AB) is;

$$AB = \frac{(ab - b) - (a - (1))}{2n} \tag{F.3}$$

For instance let us say the following experiment shown in Figure F.2 is carried out and the values are obtained. Herein;

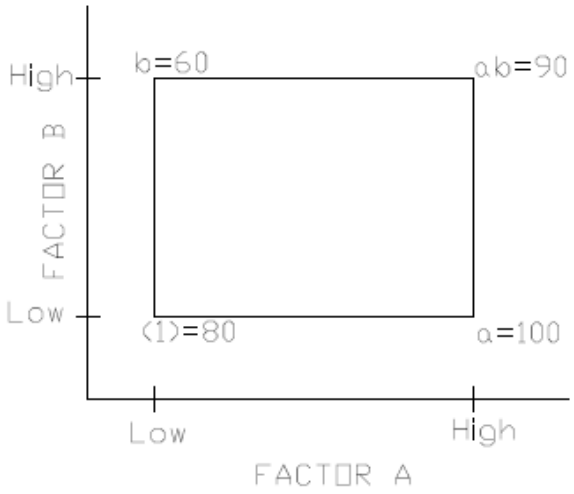

Figure F.2 A Numerical Example of Treatment Combinations in 2^2 Design

We may estimate the average effects as, n=1:

$$A = \frac{a+ab}{2} - \frac{(1)+b}{2} = \frac{90+100}{2} - \frac{60+80}{2} = 8.33$$

$$B = \frac{b+ab}{2} - \frac{(1)+a}{2} = \frac{90+60}{2} - \frac{100+80}{2} = -5.00$$

$$AB = \frac{(ab-b)-(a-(1))}{2} = \frac{(90-60)-(100-80)}{2} = 1.67$$

The effect of A is positive; this suggests that increasing A from the low level to the high level will increase yield. The effect of B is negative; this suggests that increasing the value of B will decrease the yield. The interaction effect appears to be small relative to the two main effects.

The 2^3 Factorial Design

In case there are there factors, say A, B and C, are of interest; the design is called "2^3 factorial design". Consequently, there exist eight treatment combinations which are to be represented as a rectangular prism, depicted in Figure F.3.

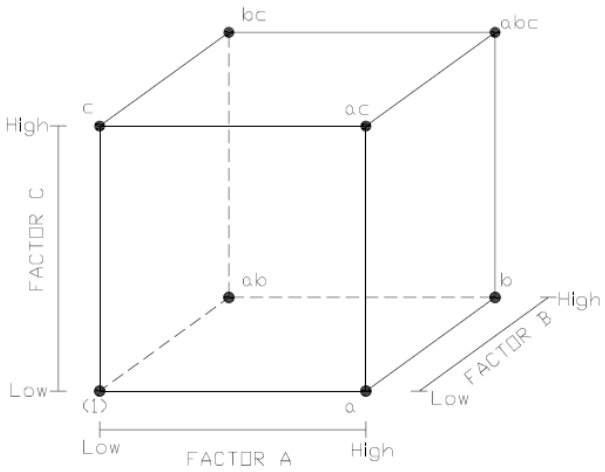

Figure F.3 Graphical Representation of a 2^3 Factorial Design

Using "+" and "-"notation represent the low and the high levels of the factors, eight runs can be listed as in Table F-1. This is called design matrix. The treatment combinations are (1), a, b, c, ab, ac, bc and abc.

There are seven degrees of freedom between the eight treatment combinations in the 2^3 factorial design. Three degrees of freedom are associated with the main effects of A, B, and C. four degrees of freedom are associated with interactions; one each with AB, AC, and BC and one with ABC [59].

Table F.1 Design Matrix

	Factors		
	A	B	C
1	-	-	-
2	+	-	-
3	-	+	-
4	+	+	-
5	-	-	+
6	+	-	+
7	-	+	+
8	+	+	+

By making use of the idea used in 2^2 factorial design, the main effects of A, B, and C are calculated as:

$$A = \frac{1}{4n}\left[a - (1) + ab - b + ac - c + abc - bc\right] \tag{F.4}$$

$$B = \frac{1}{4n}\left[b + ab + bc + abc - (1) - a - c - ac\right] \tag{F.5}$$

$$C = \frac{1}{4n}\left[c + ac + bc + abc - (1) - a - b - ab\right] \tag{F.6}$$

A measure of the AB interaction is the difference between the average A effects at the two levels of B. By convention one-half difference is called AB interaction [59].

A effect at the high level of B:

$$\frac{[(abc - bc) + (ab - b)]}{2n} \tag{F.7}$$

A effect at the low level of B:

$$\frac{[(ac-c)+(a-(1)]}{2n} \tag{F.8}$$

The difference between these:

$$\frac{[abc-bc+ab-b-ac+c-a+(1)]}{2n} \tag{F.9}$$

Similarly;

The effect of AC interaction:

$$AC=\frac{[(1)-a+b-ab-c+ac-bc+abc]}{4n} \tag{F.10}$$

The effect of BC interaction:

$$BC=\frac{[(1)+a-b-ab-c-ac+bc+abc]}{4n} \tag{F.11}$$

the ABC interaction is defined as the average difference between the AB interaction for the two different levels of C [59]. Thus,

$$\begin{aligned} ABC &= \frac{1}{4n}[(abc-bc)-(ac-c)-(ab-b)+(a-(1))] \\ ABC &= \frac{[abc-bc-ac+c-ab+b+a-(1)]}{4n} \end{aligned} \tag{F.12}$$

The quantities in the brackets in numerators are called contrasts in the treatment combinations. Using these contrasts the Table F.2 is developed with plus and minus signs [59].

Table F.2 Signs for Calculating Effects in 2^3 Design [59]

	Factorial Effect						
Treatment Combination	A	B	AB	C	AC	BC	ABC
(1)	-	-	+	-	+	+	-
a	+	-	-	-	-	+	+
b	-	+	-	-	+	-	+
ab	+	+	+	-	-	-	-
c	-	-	+	+	-	-	+
ac	+	-	-	+	+	-	-
bc	-	+	-	+	-	+	-
abc	+	+	+	+	+	+	+

Linear Regression Model for 2^3 Factorial Design

In the linear regression model, the main effects are expressed as x_1, x_2, x_3 and the interaction effects are represented as x_1x_2, x_1x_3, x_2x_3 and $x_1x_2x_3$. The variable coefficients of these terms are β_1, β_2, β_3, β_{12}, β_{13}, β_{23} and β_{123}. As a result the model is written as;

$$y = \beta_0 + \beta_1 x_1 + \beta_2 x_2 + \beta_3 x_3 + \beta_{12} x_1 x_2 + \beta_{13} x_1 x_3 + \beta_{23} x_2 x_3 + \beta_{123} x_1 x_2 x_3 + \varepsilon \quad \text{(F.13)}$$

By substituting the interaction effects with, $x_1x_2=x_4$, $x_1x_3=x_5$, $x_2x_3=x_6$, $x_1x_2x_3=x_7$ and substituting their variable coefficients with $\beta_{12}= \beta4$, $\beta_{13}= \beta5$, $\beta_{23}=\beta6$ and $\beta_{123}= \beta7$, the equation can be expressed as [59]

$$y = \beta_0 + \beta_1 x_1 + \beta_2 x_2 + \beta_3 x_3 + \beta_4 x_4 + \beta_5 x_5 + \beta_6 x_6 + \beta_7 x_7 + \varepsilon \quad \text{(F.14)}$$

The coefficients in the model are calculated as

$$\beta = (X'X)^{-1}X'y \tag{F.15}$$

APPENDIX G

MEASUREMENT SAMPLES

The measurements taken from the specimen which was cut with a cutting speed of 90 m/min, a depth of cut of 1 µm and a feedrate of 1 mm/min are given in Figures G.1, G.2 and G.3.

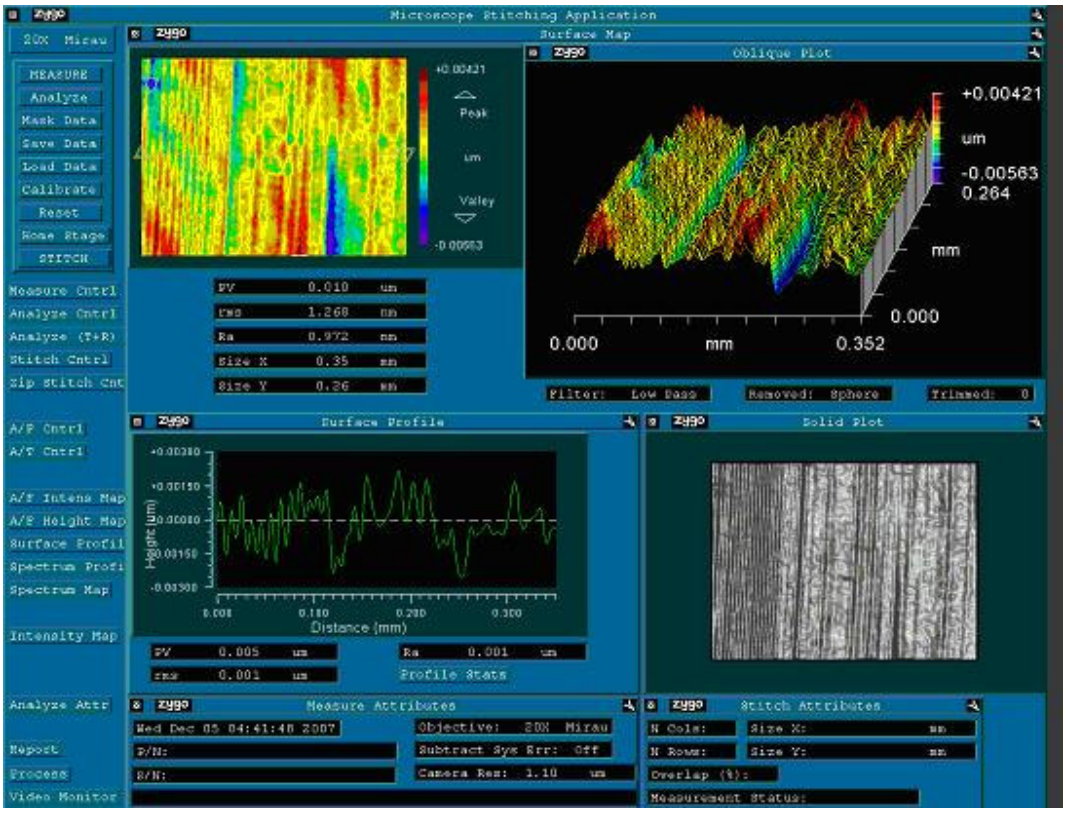

Figure G.1 A View of Output Window for Measurement 1 (V=90 m/min, d=1 µm, fr=1 mm/min)

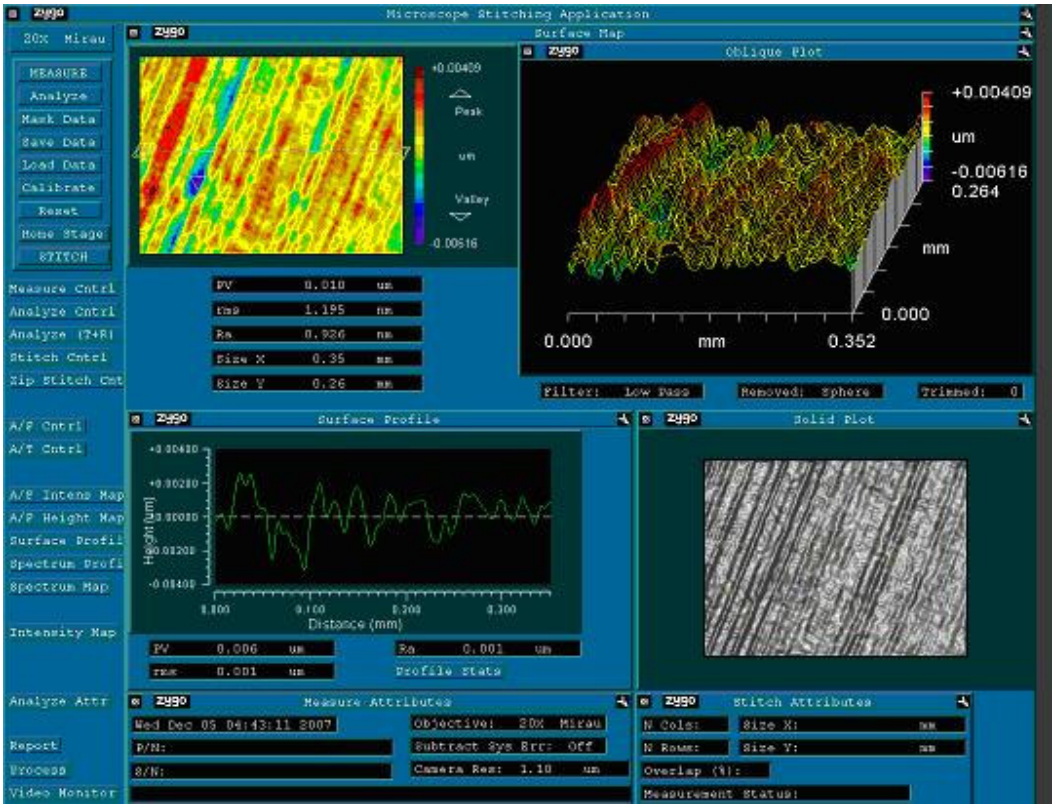

Figure G.2 A View of Output Window for Measurement 2 (V=90 m/min, d=1 µm, fr=1 mm/min)

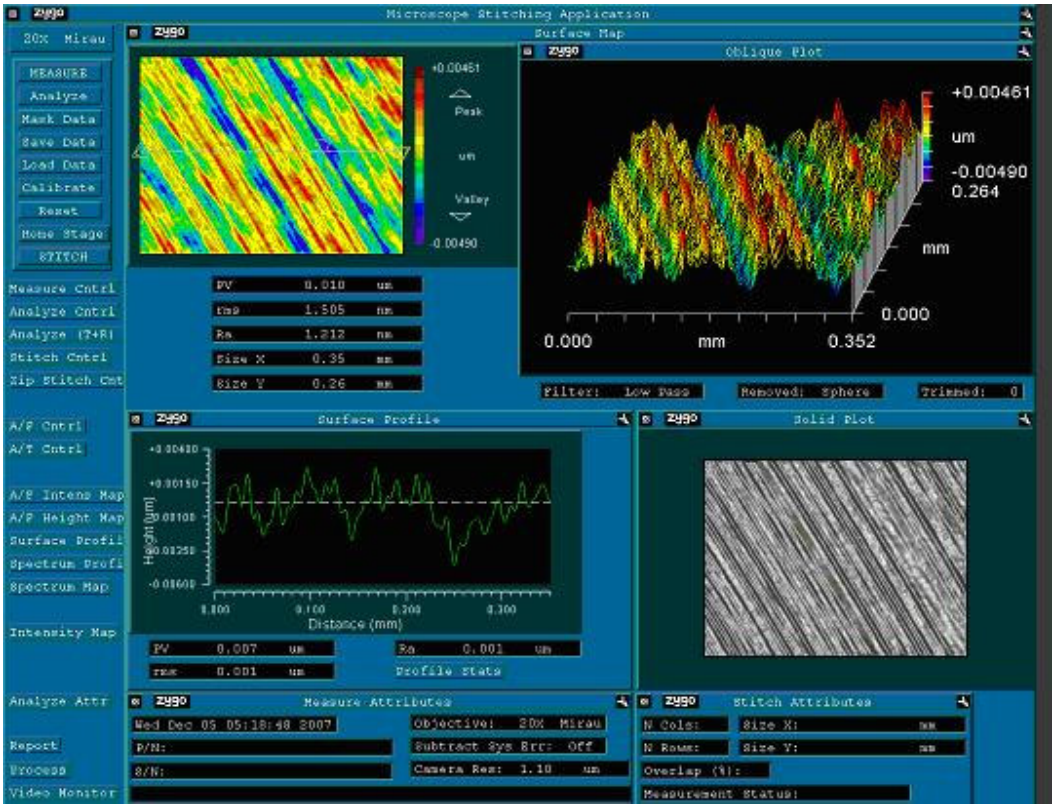

Figure G.3 A View of Output Window for Measurement 3 (V=90 m/min, d=1 µm, fr=1 mm/min)